This is the final draft of the contribution published as:

Huang, Y., **Shao, H.**, Wieland, E., **Kolditz, O.**, Kosakowski, G. (2018):
A new approach to coupled two-phase reactive transport simulation for long-term degradation of concrete
Constr. Build. Mater. **190** , 805 – 829

The publisher's version is available at:

http://dx.doi.org/10.1016/j.conbuildmat.2018.09.114

A new approach to coupled two-phase reactive transport simulation for long-term degradation of concrete

Yonghui Huang[1,2], Haibing Shao[2,5,*], Erich Wieland[3], Olaf Kolditz[2,4] and Georg Kosakowski[3]

[1] Key Laboratory of Shale Gas and Geoengineering, Institute of Geology and Geophysics, Chinese Academy of Sciences, Beijing 100029, China

[2] Department of Environmental Informatics, Helmholtz Centre for Environmental Research – UFZ, Permoser Straße. 15, 04103 Leipzig, Germany

[3]Laboratory for Waste Management, Paul Scherrer Institute, 5323 Villigen PSI, Switzerland

[4]Applied Environmental Systems Analysis, Dresden University of Technology, Germany

[5]Freiberg University of Mining and Technology – TUBAF, Gustav-Zeuner- Straße 1, 09596 Freiberg

Correspondence to: Haibing Shao (haibing.shao@ufz.de)

Abstract We present a new model for fast and efficient simulation of long-term concrete degradation due to alkali-silica reaction (ASR) and carbonation. The novel model provides an alternative coupling solution of reactive transport and multiphase multi-component flow by approximating the complex chemical reactions into a quickly calculating look-up table, which can further be integrated into a two-phase multi-component transport model via source/sink terms. The complex dynamic interplay between chemistry and multi-phase transport are well addressed in this approach. A 1-D reactive transport benchmark is proposed by taking into account the two main chemical reactions which drive the concrete degradation: ASR and carbonation caused by transport of CO_2 in a gas phase. We contrast three different sets of simulations to explore the pattern of competition between ASR and carbonation in the

long-term degradation of concrete. The numerical model derived from the look-up table approach is compared to a full reactive transport code to validate its accuracy and efficiency. It is shown that the look-up table approach and the full reactive transport code produce very similar results for degradation of concrete even for the case of competition between ASR and carbonation. However, in terms of performance, it is observed that the look-up table approach leads to a considerable reduction in calculation time. Future work will be focused on incorporating the proposed model with a geo-mechanical model for multi-chemo-physics analysis of the concrete evolution.

Keywords: concrete degradation, carbonation, ASR, multiphase reactive transport modelling, look-up table

1 Introduction

In the field of nuclear waste disposal research, the long-term stability and properties of cement-based materials is of great importance with the aim of ensuring safe disposal over very long time periods [1]. Cement-based materials have been used for several decades for the conditioning of specific waste types (e.g. [2]). The materials are also important components of the engineered barrier system of the planned deep geological repositories for low- and intermediate-level radioactive waste in Switzerland [3]. Therefore, characterizing the long-term evolution of such materials is a topic of great interest, and thus receives continuous attention by the scientific community (e.g. [1], [4], [5]). The spatial and temporal evolution of cementitious materials in a deep geological repository is influenced by several external and

internal processes involving chemical reactions and water/humidity transport, which are usually tightly coupled with each other [6,7].

In the Swiss disposal concept, the use of cement-based materials shall provide a stable mechanical and a high pH chemical environment throughout the repository for a very long period. Highly alkaline conditions are favorable as the sorption of radionuclides is enhanced on cement phases in these conditions and further corrosion of metals and microbial degradation of organic wastes is decelerated. The two latter processes limit gas generation. The long-term chemical stability of cement materials is further of great importance because in the course of cement/concrete degradation, cement phases are successively dissolved which reduces the pH buffering capacity of cement paste and results in a continuous drop in pH with time (e.g. [7,8]). Once the chemical environment evolves to near-neutral conditions, gas production and water consumption in the repository could be considerably accelerated due to the significantly enhanced rates for metal corrosion and degradation of organic wastes in these conditions.

In the Swiss concept, repositories for radioactive waste are foreseen to be built in tight clay rocks. Their low permeability limits exchange of gases, water and dissolved components between the repository and the host rock. Over time, considerable amount of gases will be produced in the repository due to the corrosion of metals and the degradation of organic waste materials. Gas production in combination with the very low permeability of the surrounding host rock is expected to allow for a very long period of partially water-saturated conditions in various parts of the repository [9]. Under such conditions, water transport and water availability in the repository is mainly driven by the humidity diffusion in the gas phase.

According to Kosakowski et al.[10], the most important processes controlling concrete degradation in a cement-based repository are the ingress of host rock pore water, concrete carbonation due to the production of CO_2 by (bio-)chemical degradation of organic wastes, internal degradation of concrete due to the use of reactive silicate aggregates, and interactions between waste materials and cement paste. Note that the latter processes involve water-consuming reactions. All these processes must be assessed in the context of a repository system to ensure the long-term safety of nuclear waste storage.

Firstly for the ingress of formation water, it is controlled by the diffusive transport across the clay/cement interface, thus its amount is considered to be very low in an intact claystone host rock with partially saturated water content. Within a period of 100’000 years, which is typical for the service life of a low- and intermediate-level waste repository, only small zones of degraded concrete are expected to occur [11].

Secondly, carbonation is of major concern in cement-based repositories. The carbonation of concrete is a well investigated phenomenon in civil engineering [12,13,14]. Current research (c.f. [15]) shows that the process is mainly controlled by the transport of gaseous CO_2, the atmospheric humidity/water saturation of the concrete, and the cement composition. It is known that the shape of carbonation fronts in cements is influenced by kinetic constraints on the reaction rates of the successive dissolution of cement phases [16]. For practical purposes, however, carbonation can be treated as an equilibrium process on the time scales relevant to waste disposal (hundreds of thousands of years). Typically, the gas diffusion coefficient is about 10’000 times greater than in water. In addition, in a cement-based repository cements are in direct contact with waste materials that serve as the sources of CO_2.

Therefore, the carbonation of concrete in a partially water-saturated cement repository is normally not limited by the diffusive transport of CO_2, but instead it largely depends on CO_2 generation.

Thirdly, internal degradation of concrete due to the presence of aggregates has a potentially detrimental effect on the cement-based engineered barrier [17]. The internal degradation of concrete due to the reaction of cement phases with aggregates is known as the alkali-aggregate reaction (AAR). The two main types of AAR are the reaction with silica-containing aggregates, the so-called alkali-silica reaction (ASR), and the reaction with dolomites, the so-called alkali-carbonate reaction (ACR) (e.g. [18]). The ASR is particularly relevant in conjunction with waste disposal, as silica aggregates are often used in the conditioning of radioactive waste [19]. In principle, quartz or silicates (SiO_2 polymorphs) are not in thermodynamic equilibrium with most cement phases. Thermodynamic equilibrium is reached upon conversion of most cement phases into calcium-silicate hydrates (C-S-H) with low calcium/silica (C/S) ratio or other silicate minerals [20]. The kinetics of the dissolution of silicate aggregates is the main factor that drives the progress of ASR. The dissolution rate depends on the specific mineral (e.g. quartz, feldspar, etc.), the reactive surface area, which is linked to the aggregate particle size, and on the pH [21]. Kosakowski et al. [6] estimated that for a backfill mortar with quartz spheres of 2.8 mm diameter, the aggregates may completely dissolve within 500 years based on the dissolution rates reported by Palandri and Kharaka [21]. There is no macroscopic transport process necessary to drive ASR, except that minimum water saturation is required in the concrete and the need for a microscopically connected water phase to allow transport of reactants from the aggregates to cement mineral grains.

Eventually, the interaction of degrading waste materials could influence the performance of the cement-based engineered barrier. For example, the corrosion products of metals, such as aluminum, steel, etc.,

could interact with cement phases and change the mineral composition of the cement paste. To date, however, these processes are only poorly known and their consequences on the evolution of barrier performance can hardly be assessed.

Numerical simulation is an efficient tool which can improve the understanding of the complex interaction and feedback between different physical and chemical processes. It also provides detailed information on the temporal and spatial evolution of water saturation and the pressure evolution in a repository [9,22–24]. Most of the current reservoir models are restricted to multi-phase transport phenomena without the consideration of feedback between the chemical evolution, water availability and gas generation. From the numerical point of view, incorporation of such feedback requires the solution of mass conservation PDEs describing the multi-phase multi-component flow, coupled with modules simulating chemical reactions and providing local rates for the mass conservation PDEs.

Over the last decade, the coupling between multi-phase multi-component flow with reactive transport has been in the focus of research. Several numerical simulators have been developed and were applied in reservoir simulations and also in the investigation of environmental and hydrogeochemical systems. The GEM-GHG [25] and GPRS [26] codes extended the original compositional multi-phase flow simulators with the chemical reactive transport by solving the coupled system in a fully implicit way. In contrast, several reactive transport simulators, e.g. CRUNCHFLOW [27], PFLOTRAN [28], STOMP [29], TOUGHREACT [30] and HYTEC [31], integrated the multi-phase flow model based on an operator-splitting approach, in which the computations for one time step are split into a flow problem and a reactive transport problem, respectively. Coupled multi-phase reactive transport is also a very active area of research in the framework of radioactive waste disposal. Leterrier and Bary [32] studied

concrete durability and proposed a reactive transport model considering transport in a partially saturated medium in combination with CO_2 diffusion in gas phase, in which the chemical reaction can be both at equilibrium or kinetically-controlled. Thouvenot et al. [33] and Trotignon et al. [34] simulated the atmospheric carbonation and drying process in low and intermediate level waste (L\ILW) disposal cells components with the TOUGHREACT code.

Given the complexity of the reactive multi-phase transport codes, as well as the high nonlinearities embedded in the coupled processes, it is evident that most codes have to deal with serious challenges related to model robustness and computational efficiency. In addition, the potential degradation of concrete material combines processes that act on very different time scales, from very fast reactions (equilibrium chemistry) to slow, kinetically-controlled processes. Meanwhile, simulating the repository evolution requires the calculation of time spans up to hundreds and thousands of years with a very fine temporal resolution. Moreover, from a chemical point of view, concrete is a complex material which mostly contains phases best described in terms of solid-solutions, e.g. C-S-H (e.g. [35] [36]). The thermodynamic setup for concrete is considered complicated which significantly enhances the numerical effort to solve the chemical problem. Therefore, the current codes and models suffer from severe limitations for the investigation of the concrete evolution, especially when applied in the context of multi-scale simulations.

De Lucia et al. [37] proposed an approach to overcome the numerical and computational problems for fine-grained, repository-scale reactive transport simulations in the field of CO_2 sequestration. The authors pre-calculated the reaction path of the reservoir rock during the exposure to CO_2 with a geochemical batch model. The exposure time to CO_2 of each element of the hydrodynamic grid was

estimated and the result of the batch geochemical model was applied to each grid element during its exposure time. This approach is a simplified one-way coupling and does not allow for feedback of the chemical model into multi-phase transport as it assumes that the chemical reactions are only driven by the presence of CO_2, and that the reactions are controlled by very slow kinetics. Therefore, the migration of CO_2 in the reservoir was only marginally affected by the chemical reactions. Nevertheless, the authors demonstrated that, for systems that obey the above constraints, a simplified reactive transport coupling provides an acceptable approach to calculate reservoir evolution with fine-grained models.

An alternative solution to these problems is to convert the chemical equilibrium calculations into a look-up table. Such an approach has been widely used in various areas such as combustion simulation or the inclusion of chemical reactions in atmospheric simulations (e.g. [38,39]). For example, Fukumoto and Ogami [40] used a pre-computed look-up table to simplify the chemical equilibrium calculation for combustion simulations. The authors reported that a 75% reduction in the overall computation time can be achieved with the look-up table approach. Further, Fiorina et al. [41] proposed tabulated chemistry methods for large eddy simulation in turbulent flow. Wang et al. [42] introduced an improved look-up table approach to fit the chemical kinetic reaction rate, which led to an accelerated calculation in atmospheric chemistry-transport simulations. In general, it has been demonstrated that the look-up table approach can be used to enable numerically efficient computations of chemical systems. More details on this approach are available from Anderson et al. [43] and Turányi and Tomlin [44].

To the best of our knowledge, no work has been reported to date on the use of the look-up table approach in combination with a multi-phase multi-component model in the field of nuclear waste

disposal. In this work, an initial attempt is being made to parameterize the concrete degradation reactions into a pre-calculated look-up table, which can then be cast into a two-phase multi-component model via source and sink term for the component water and gases. In contrast to previous efforts, the computation of the chemical reaction in the course of a simulation becomes a procedure without numerically solving the chemical system. The complex chemical solver can be replaced by a call to the look-up table, which has the additional advantage that the look-up table provides derivatives of properties with minimal numerical costs. Moreover, this method allows the use of existing numerical simulators of multi-phase multi-component models to simulate the complex coupled problem without the need of excessive modification of the simulator structure.

This paper presents an extension of the multi-phase multi-component transport code OpenGeoSys-MP [45] with a look-up table describing the degradation of concrete due to carbonation and ASR. OpenGeoSys-MP is part of the open-source platform OpenGeoSys [46] in which reactive transport codes have been developed for both operator-splitting via code coupling [47–50] and global-implicit approaches [51]. The paper is organized as follows: first, the chemical model for concrete degradation and the approximation by the look-up table is explained (**Sect. 2**). The section is followed by the description of the physical model of two-phase, multi-component flow coupled with reactive transport (**Sect. 3**). The validation of the proposed look-up table approach is presented in **Sect. 3.2**, in which three different benchmarks are proposed and the numerical results are analyzed. After detailed discussions in **Sect. 4**, S**ection. 5** is dedicated to summarizing the conclusions and outlook.

.

2 The mathematical, chemical and physical framework

2.1 Concrete degradation and creation of look-up table

The look-up table approach described in this work is very flexible, as it is possible to tune the look-up table to represent a specific concrete. This also implies that one "generic" look-up table does not exist and that for each material a separate look-up table has to be created. In this work, the look-up table is calculated based on the thermodynamic model of a sulfate-resisting Ordinary Portland Cement (OPC), similar as the one described by Lothenbach and Wieland [52]. The exact recipe and the detailed thermodynamic setup of the utilized concrete are given in Wieland et al. [53]. Only the most important information is explained in this work.

The normative composition of the concrete is given in Table 1. The setup represents a typical mortar used for backfilling void space in waste packages. All calculations were conducted with the GEM-Selektor V3 chemical modelling package [54,55] based on the PSI/Nagra thermodynamic database [56], the CEMDATA V07.03 [57] for cement phases and the Thermoddem database [58] for clay and zeolite minerals. In the thermodynamic modeling and the chemical setup of the system the alkalis are taken into account and solution concentrations and the distribution between alkali-containing solids have explicitly been modelled. Thermodynamic models have been implemented to mimic the uptake of the alkalis by calcium-silicate hydrates (C-S-H phases), zeolites, i.e. Analcime, Chabazite, K- and Na-phillipsite). The model for C-S-H is based on the solid solution model of Kulik and Kersten[59] and is extended to account for alkali uptake as described in X. Gaona et al. [60]. Concerning the concentration of the anionic counterions it is to be noted that OH- is the main anion in all modeling set-ups. Very high Cl-

concentrations are only achieved for special degradation scenarios (e.g. ingress of sea water or brines) which are not relevant in connection with the present modeling study. The thermodynamic setup with complete component list is given in Appendix B.

205

Table 1: Setup and properties of generic mortar.

Phase/Material	amount [g]	Remark
Water (H_2O)	169.25	
CEM I 52.5 N HTS[1]	300	Corresponding composition is given in Appendix A.
NaCl	0.1	Represents small amount of salts in the water
Aggregate (SiO_2/quartz)	1830	For the initial equilibration, aggregate is assumed to be not reactive
total mass (compare with Table 2)	2299.35 g	
W/C ratio (adjusted to give a porosity of 0.076)	0.564	Wieland et al. [53] considered an additional gas phase, here fully saturated conditions are assumed

[1] Cement classification: CEM I 52.5 N; HTS = haute teneur en silice

- **Hydrated mortar**

The calculated equilibrium composition for the fully hydrated mortar is given in Table 2. The equilibrated composition is very similar to the concrete used by Kosakowski and Berner [61], with the only difference that hydrogarnet replaces monocarbonate. Due to the inclusion of alkali uptake on C-S-H, the calculated pH is about 12.9, which is lower than the original pH reported by Kosakowski and Berner [61]. Also, the calculated pore water properties are slightly different because in Kosakowski and Berner [61] a different water composition was used to set up the concrete.

The equilibrated mortar is the starting composition for the degradation calculations that span the look-up table. Only two degradation reactions have been considered for this work: the alkali-silica reaction (ASR) and the carbonation. Both reactions successively dissolve calcium-bearing cement phases to form carbonates in case of carbonation or C-S-H with low C/S ration, and/or silica gel, in the case of ASR. The progress of both processes was calculated with the help of the sequential batch module of the GEM-Selektor V3 software. The initial hydrated system was scaled such that it corresponded to a volume of 1e-3 m^3 (1 litre).

Table 2: Calculated phase composition of hydrated concrete

Composition/phase	Amount [g]	Amount [mol]	Volume fraction [-]
aq_gen[1]	71.151	3.942	0.076282
C3(AF)S0.84H - hydrogarnet (solid solution)	30.695	0.144	0.01125
ECSH2 - C-S-H (solid solution)	204.103	1.703	0.08724

barite	0.00898	3.847e-05	2.156e-6
ettringite	34.467	0.0275	0.02089
calcite	10.916	0.109	0.0043333
portlandite	105.813	1.428	0.05079
magnetite	8.628e-06	3.726e-08	1.691e-9
OH-hydrotalcite	7.012	0.0158	0.00374686
aggregate + inert cement phases (represented by inert quartz)	1835.184	30.543	0.745466

total mass (compare with Table 1)	2299.35 g
total volume	929.582 cm^3
pH	12.88
ionic strength of solution	0.129 mol/kg
Temperature	298.15 K
Eh	-0.414 V

[1]aq_gen: the generated aqueous phase.

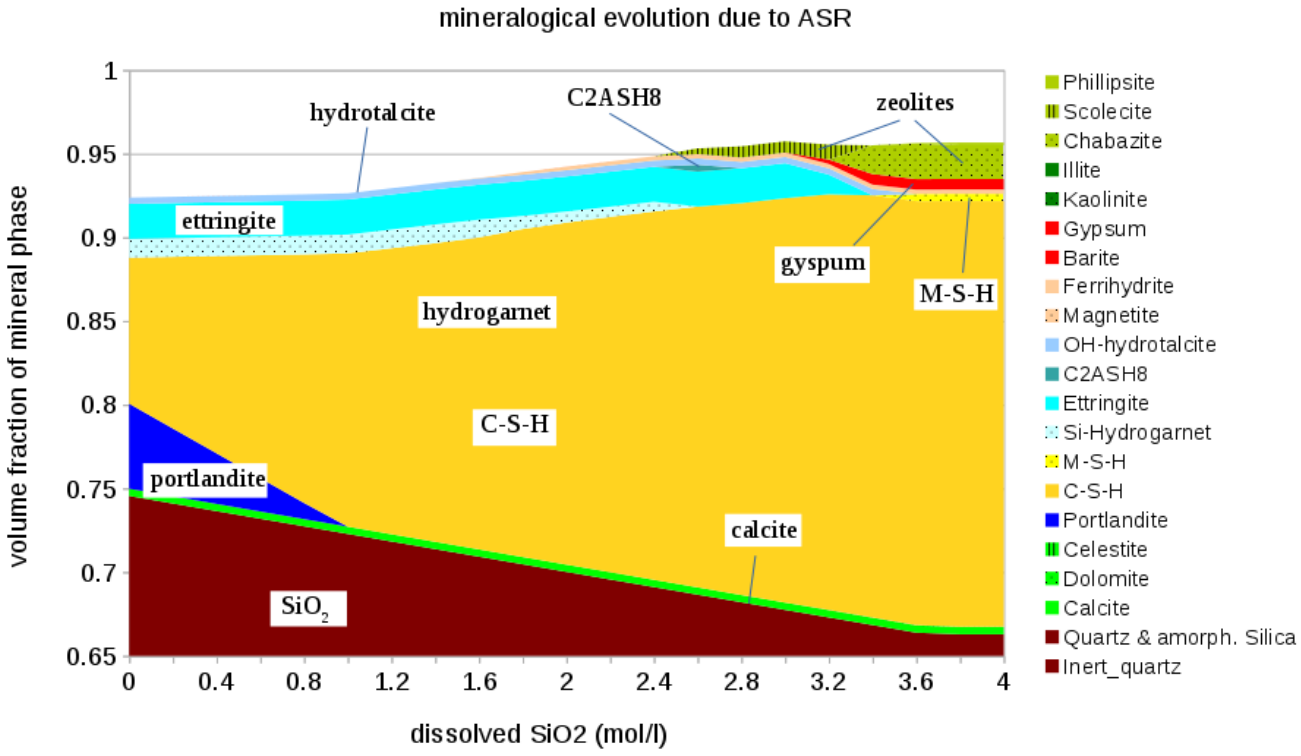
- **Carbonation**

Increasing amounts of CO_2 were added to the chemical system to model cement carbonation. After each step the system was equilibrated and the result of the GEM-Selektor calculation was saved. Figure 1-(a) shows the simulated evolution of cumulative mineral phase volume fractions along with the increasing amount of CO_2. The volume fraction of the fluid phase is not included in this plot. Initially all solid

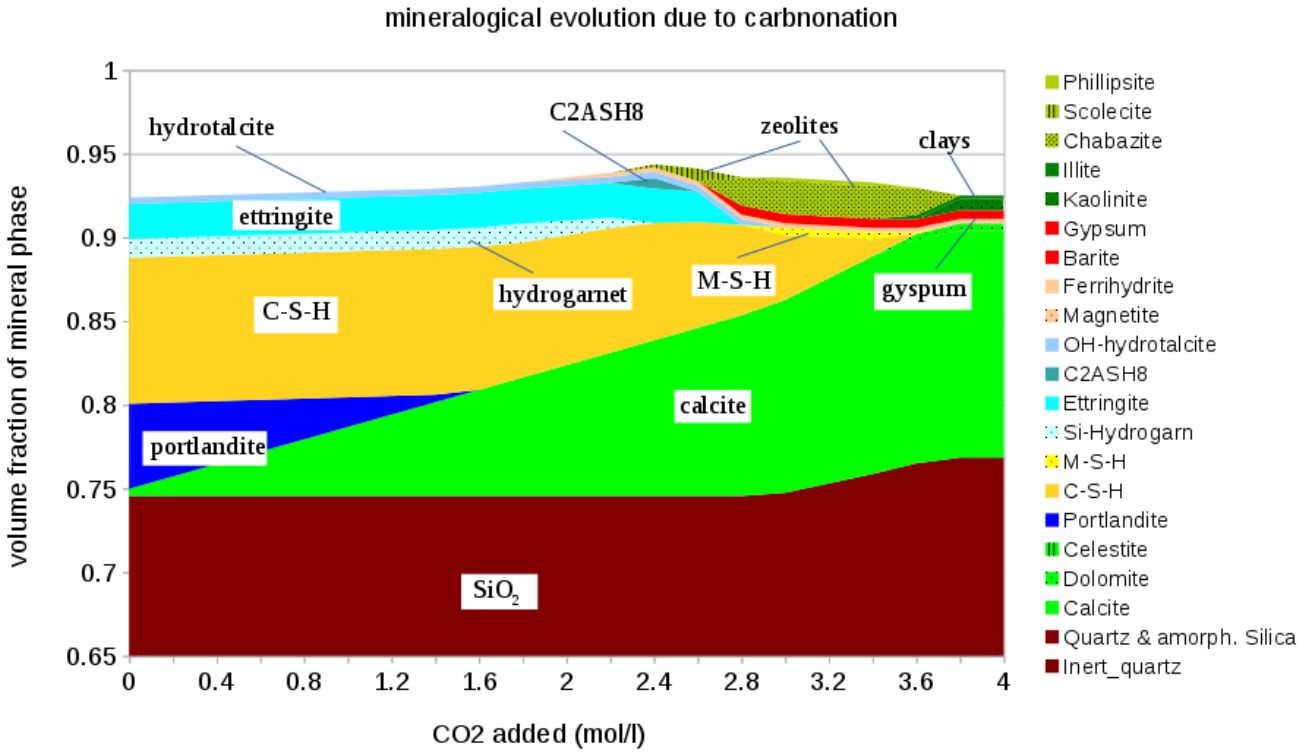
phase volumes and the fluid phase volume add up to 1. The difference between the sum of volume fractions of all solid phases and 1 can be interpreted as the porosity, i.e. the volume fraction that can be filled with gas/water. Note that the quartz aggregate is largely the dominating phase with a volume fraction of about 0.75. With the addition of CO_2, portlandite is first dissolved and transformed into calcite according to the following reaction:

$$Ca(OH)_2 + CO_2(aq) \Leftrightarrow CaCO_3(s) + H_2O$$

Through this reaction water is released. After portlandite is consumed, C-S-H phases with a high C/S ratio are transformed into C-S-H with low C/S. The utilized model for C-S-H has a minimum C/S ratio of 0.8 (tobermorite as the end-member of the solid-solution). This transformation also frees water. Once all calcium has been leached from the C-S-H phases as a consequence of the reduction of the C/S ratio, successively hydrogarnet, ettrringite, hydrotalcite and C-S-H with the lowest possible C/S ratio are dissolved. The leached calcium is used to form calcite. The dissolution of the AFm and AFt phases also releases aluminium which serves as the basis to form zeolites. Ettringite dissolution leads to the formation of sulfates, in this case gypsum, and magnesium is used up due to the transformation of C-S-H into M-S-H (Magnesium silicate hydrates). Excessive silica resulting from the C-S-H dissolution gives rise to the precipitation of SiO_2, which is shown in the model as the formation of amorphous silica or quartz. The final, completely carbonated system is composed of largely unaffected quartz aggregates, considerable amounts of carbonates and minor amounts of clay minerals. This last degradation stage is a fictive stage only based on thermodynamic equilibria. Whether this stage will be reached in reality is uncertain, as the formation of clay minerals under repository conditions is highly controversial because it is likely to be a slow process.



(a) Mineralogical evolution due to carbonation



(b) Mineralogical evolution due to ASR

Figure 1: Mineralogical evolution of concrete during carbonation in terms of volume fractions while adding successive amounts of CO_2 to the system (a). Mineralogical evolution of concrete during ASR in terms of volume fractions while reacting successive amounts of the (dissolved quartz) aggregate (b) (lower figure).

- **ASR**

In our thermodynamic setup, the ASR is mainly driven by the dissolution of the quartz aggregates. The released silica reacts with calcium leached from the cement phase to form C-S-H solid solutions. As a consequence of progressing silica release, silica is continuously bound by C-S-H; therefore, the C/S ratio of the C-S-H phase decreases towards 0.8, the C/S ratio of the tobermorite ($SiO_2(Ca(OH)_2)_{0.8}H_2O$) as the end-member of the C-S-H solid solution model. It should be noted that, at the present time, no

thermodynamic data are available for the ASR product whose structure has recently been disclosed (Dähn et al., [62]). As a consequence of missing thermodynamic data, the ASR is not implemented as alkali-containing phase, which certainly is a simplification of the real situation. In our simplified modeling approach C-S-H phases are considered to be the main product of the ASR. The general sequence of dissolving cement minerals (Fig. 1-(b)) and precipitated secondary phase is very similar to the carbonation reaction, except for the two main differences: firstly, during carbonation, C-S-H is dissolved and carbonates are formed, whereas for ASR, carbonates do not participate in any reactions and C-S-H is the main reaction product. Secondly, for the ASR, zeolites will be transformed to clay phases in the very last degradation stage. Such transformation is not present in the carbonation reactions.

- **Chemical and physical changes upon cement degradation**

The combined effects of carbonation and ASR on pH in pore water, on porosity, water volume and quartz dissolution rate are shown in Fig. 2.

The pH in the system decreases during concrete degradation, for both carbonation and ASR. In the initial hydrated concrete, the pH is 12.9 whereas the pH of degraded concrete only reaches 10.1. At the final degradation stage by carbonation, the pH drops further to 8.3 as a consequence of the presence of clay phases.

The quartz dissolution rate was calculated as described by Wieland et al. [53] for sand grains with 1.5 mm diameter and for a unit system volume of $1 \cdot 10^{-3}$ m^3. The dissolution kinetics of siliceous sand

(aggregate) can be expressed in terms of a (simplified) pH-dependent rate in accordance with [10] which includes neutral and alkaline mechanisms:

$$R_{diss} = \frac{\mathrm{dm}}{\mathrm{dt}} = A \cdot \left(k_1(1-\Omega) + k_2 \cdot a_{H^+}^{-0.5}(1-\Omega)\right) \quad \left(\mathrm{mol\ s^{-1}}\right), \tag{1}$$

A: reactive surface area (m^2) $A = A_S \cdot M$ with

M: mole amount of the siliceous sand present

A_S: the specific surface area for a porous medium filled with spherical quartz grains of 1.5 mm diameter

A_S = 0.091 (m^2 mol^{-1})

k: rate constants for neutral and alkaline mechanisms (mol s^{-1} m^{-2})

log k_1 = -13.99; log k_2 = -16.29

a_{H^+}: activity of hydrogen ion

Ω: saturation index

The above rate equation was taken from the compilation of dissolution rates by Lasaga and co-workers [63–65]. The reactive surface area was held constant as for complete degradation, only about 10% of the overall siliceous aggregate was consumed. As the pH is a (logarithmic) measure of hydrogen ion activity, the rate law exhibits very strong pH dependence, i.e. at high pH values the dissolution of quartz is highly accelerated.

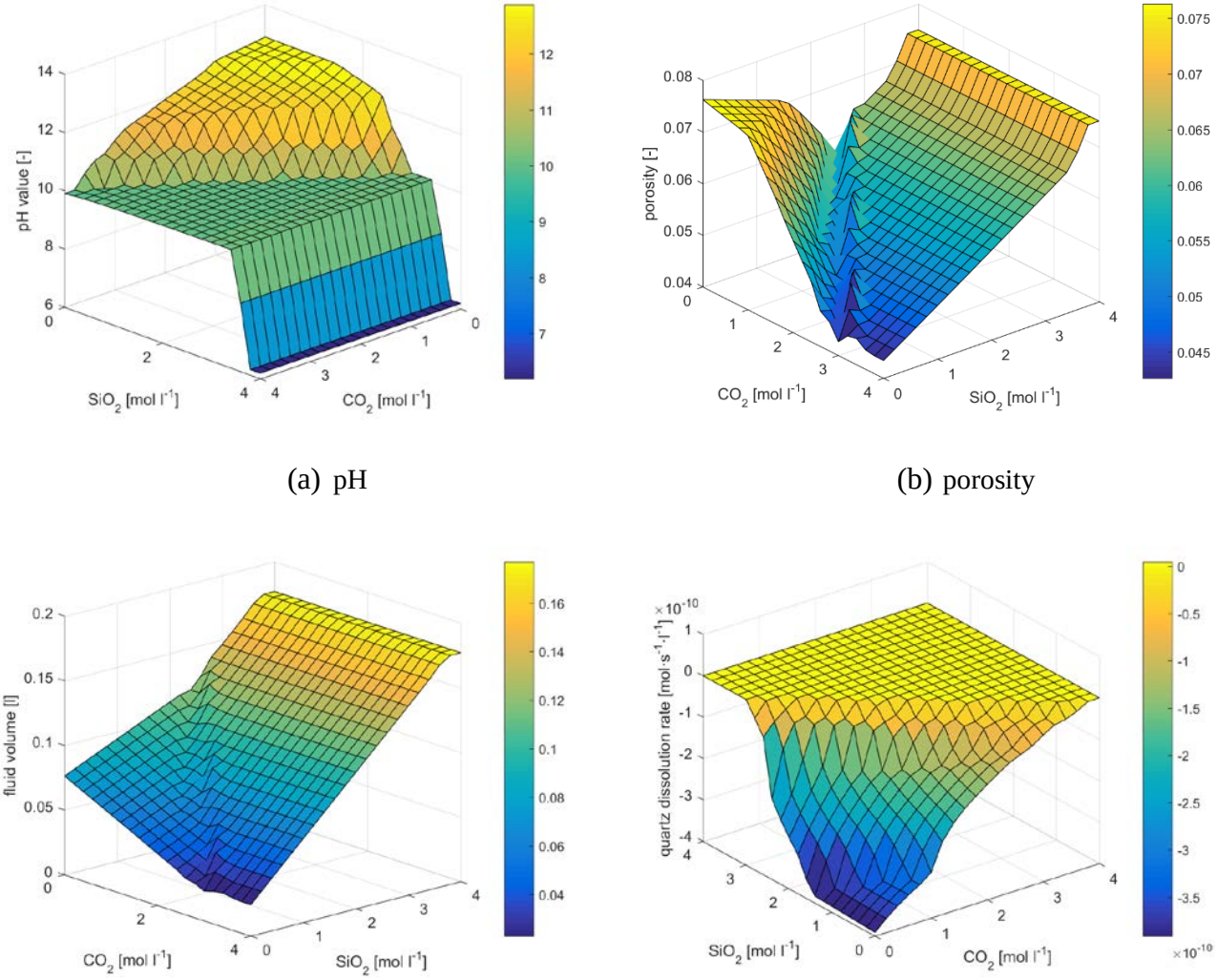
A look-up table was constructed with the help of process simulator module of GEM-Selektor. The process simulator uses a scripting engine to control equilibration of chemical systems based on varying input composition. The scripting engine allows the automatic calculation of titration, phase diagrams,

batch reactions or even simple transport calculations. We wrote a script that re-equilibrates the hydrated mortar from Table 2 after adding a defined amount of CO_2 and allowing the dissolution of a specific amount of aggregate (SiO_2). The initial system from Table 2 was scaled to represent a volume of 1 litre. All calculations were carried out at a temperature of 298.15 K（25 °C）and a pressure of 1 bar.

For the re-equilibrated system various properties like pH, volume of all solid phases, volume of the liquid phase, saturation indices for mineral phases were extracted and stored in a table. Using Equation 1, the dissolution rate was calculated for a specific equilibrated system and also stored. For such a setup, where temperature and pressure are constant and no water is added or removed from the overall system, the volume of the liquid phase changes according to its composition and according to consumption/release of water due to mineral transformations.

The entries in the look-up table were calculated from 0 mol to 4 mol with a step size of 0.2 mol for adding CO_2 and dissolving SiO_2. This results in $21 \times 21 = 441$ sampling points in the table. From all the possible properties of the equilibrated system only some information was included in the look-up table. Two input columns contain the added amount of CO_2 and dissolved SiO_2. Four output columns contain the values for pH, porosity (initial volume divided by actual volume of all solids), liquid volume and quartz dissolution rate. Additionally, two extra columns are attached to indicate if ASR and carbonation are complete. ASR is assumed to be complete once the aggregate (quartz) is in thermodynamic equilibrium with the other mineral phases, or if quartz is oversaturated and would precipitate. Carbonation is assumed to be complete once the added CO_2 is not completely consumed for mineral transformations.

Within OGS-MP-LT the interpolation to intermediate values is carried out by the bilinear interpolation scheme. All the gradients are calculated using numerical differentiation, such as finite difference method. After the reaction of the corresponding moles of SiO_2 and CO_2, the volume of the liquid phase was calculated and was used as the source/sink terms for liquid in the governing equation of multi-phase transport process. The difference in fluid volume before and after adding CO_2 and SiO_2 revealed the amount of mass added into or subtracted from the liquid volume. In case of a negative value, water was removed due to chemical reactions (mainly ASR). With a positive one, however, water was released, mainly by carbonation. The porosity was calculated based on the changes of cumulative solid phase volume fractions with respect to the initial volume. The porosity surface in Fig. 2 shows some local maxima at intermediate degradation stages. They are caused by the formation of intermediate phases with a low density, mainly zeolites. These phases have only a small window of stability in terms of silica or carbonate addition. Thermodynamic data for zeolite phases have relatively large uncertainties [66]. Therefore, the position and extension of these porosity changes are uncertain and strongly depend on the mineral phases included and the adopted thermodynamic data.



(a) pH

(b) porosity

(c) fluid volume

(d) quartz dissolution rate

Figure 2: 3D surface plots for the combined effects of CO_2 addition (carbonation) and SiO_2 addition (ASR) on pH (a), porosity (b), fluid volume (c) and quartz dissolution rate (d).

2.2 Coupling the look-up table with two-phase multi-component transport model

After the successful construction of a look-up table, it is coupled to the two-phase multi-component transport code OpenGeoSys-MP as described in detail elsewhere [45]. The two-phase multi-component reactive transport model is integrated into the OpenGeoSys simulation framework V.6 [67] and abbreviated throughout this work as OpenGeoSys-MP-LT or OGS-MP-LT. For the two-phase module in OGS, the standard Galerkin finite element method is employed for spatial discretization, with a fully implicit backward Euler scheme for the time integration. Application of these space and time discretization schemes to the governing equations leads to a coupled system of discrete residual equations with high nonlinearity. The Newton method with line search scheme is employed for the linearization, while a GMRES solution strategy with ILUT preconditioning is applied to solve the linear equation system.

For our application the concrete materials were conceptualized as porous media, in which the following transport equations including one gas and one liquid phase, were solved for water, water vapor and multiple gas components. This is implemented in a two-phase compositional flow model based on the generalized Darcy law in combination with diffusive transport as given by Fick's law. The mass conservation which is assumed for each component reads:

$$\frac{\partial}{\partial t}\sum_{\alpha\in\{G,L\}}\left(N_\alpha S_\alpha x_\alpha^i\right)+\nabla\left[\sum_{\alpha\in\{G,L\}}N_\alpha\left(x_\alpha^i\boldsymbol{q}_\alpha+\boldsymbol{J}_\alpha^i\right)\right]=F^i. \quad (2)$$

Here let $\alpha\in\{G,L\}$ denote the set of gas and liquid phases, x_α^i is the molar fraction of component i in phase α, S_α is the saturation of phase α, and N_α represents the phase molar density. For a particular phase α, its Darcy velocity $\boldsymbol{q}_\alpha$ is given by the generalized Darcy's law:

$$\boldsymbol{q}_\alpha = -\frac{\mathrm{K}k_{r\alpha}(S)}{\mu_\alpha}(\nabla P_\alpha - \rho_\alpha \boldsymbol{g}) , \quad (3)$$

with ρ_α indicating the mass density of phase α. The diffusive flux $\boldsymbol{J}_\alpha^i$ governed by Fick's law is given:

$$\boldsymbol{J}_\alpha^i = -D_e \nabla x_\alpha^i , \quad (4)$$

Where D_e indicates the effective diffusion coefficient.

The dissolution of the gases into the pore water is described by Henry's law:

$$x_L^i = \frac{\mathrm{H}}{\rho_L P_G^i} , \quad (5)$$

where H is the temperature dependent Henry constant. P_G^i is the partial pressure of component i in the gas phase.

The evaporation of liquid water into water vapor is described by the Raoult's law:

$$x_G^i = \frac{P_{sat}}{P_G^w} , \quad (6)$$

where P_{sat} is the saturation pressure, which corresponds to the vapor pressure of the pure water at temperature T, and it is further dependent on the temperature:

$$P_{sat}(T) = P_0 \exp\left(\left(\frac{1}{T_0} - \frac{1}{T}\right) \cdot \frac{M^w h_{\mathrm{wg}}}{R}\right) , \quad (7)$$

P_0 and T_0 are the reference pressure and temperature, respectively. h_{wg} is the specific latent heat of water vaporization.

Aqueous and gaseous components diffuse with an effective diffusion coefficient D_e that depends on the phase diffusion coefficient D_α, as well as the porosity ϕ and phase saturation S_α of the porous medium:

$$D_e = \phi S_\alpha D_\alpha \,, \tag{8}$$

Note that for each phase α, the diffusion coefficient D_α shall be identical for all components in this phase to preserve the consistency of system [68].

The Darcy velocities of liquid water and gaseous species are given by Eq. (3), taking into account the capillary pressure. In this work, the van Genuchten model [69] was adopted to describe the capillary pressure-saturation relationship:

$$P_c(S_e) = -P_r\left(S_e^{-\frac{1}{m}} - 1\right)^{\frac{1}{n}}, \tag{9}$$

where S_e indicates the effective saturation $S_e = \frac{S_L - S_{lr}}{1 - S_{lr} - S_{gr}}$ with S_{lr} and S_{gr} representing the residual saturations. P_r is a characteristic pressure for the van Genuchten model.

The relative permeability of the porous media can be expressed based on the van Genuchten model as well. For the liquid phase, the relative permeability is given as:

$$k_{rl}(S_e) = \sqrt{S_e}\left[1 - \left(1 - S_e^{\frac{1}{m}}\right)^m\right]^2, \tag{10}$$

while for the gas phase the relative permeability is given as:

$$k_{rg}(S_e) = \sqrt{(1 - S_e)}\left[1 - S_e^{\frac{1}{m}}\right]^{2m}. \tag{11}$$

A Carman-Kozeny [70] type relationship was applied to relate intrinsic permeability and porosity changes:

$$K = \mathrm{K}_0 \frac{(1-\phi_0)^2}{(1-\phi)^2}\left(\frac{\phi}{\phi_0}\right)^3, \quad (12)$$

K_0 and ϕ_0 are the initial permeability and porosity, respectively, while K and ϕ represent the updated permeability and porosity.

395

2.3 The coupling strategy

The coupling strategy for the approximation of a subset of chemical reactions and two-phase multi-component transport processes is shown in Fig. 3. For concrete materials, concrete degradation was approximated by a look-up table as described in Sect. 2. The table provides pH, porosity, water
400 consumption/release and kinetic rates for dissolution of (quartz) aggregate on dependence of CO_2 and SiO_2 reacted in a unit volume. Carbonation was calculated based on the cumulated amount of CO_2 that reaches on a node/volume by transport, while ASR was calculated based on the dissolution of SiO_2 with the kinetic rates provided by the look-up table.

Our approach for incorporating the look-up table into the two-phase multi-component transport model
405 was accomplished via source/sink term and updates of porosity and pH values on each integration point. The source/sink term was added to the right-hand side of Eq. (2) representing the production/consumption rate of one particular component due to chemical reactions. For each Newton iteration a call was made to the look-up table to define the desired values at each integration point.

The accumulated amounts of consumed CO_2 and dissolved SiO_2 for a specific integration point are
410 given as input values to a bilinear interpolation routine which extracts the chemical system information from the look-up table.

For the first Newton iteration of a time step, the accumulated consumed CO_2 and dissolved SiO_2 values from the last time step are taken.

In detail, the coupling procedure is constituted by the following steps:

1. The volumetric concentration of CO_2 is calculated on each integration point within each Newton loop. The CO_2 consumption rate is calculated under the assumption that the total amount of CO_2 that reaches an integration point shall be consumed as long as carbonation reaction is not complete. The consumption rate is then applied as the sink term to the mass conservation equation (i.e. Eq. (2)) in terms of the CO_2 component. After each Newton iteration, the accumulatively consumed CO_2 concentration is updated based on the consumption rate for the specific time step.

2. The current fluid volume can be directly obtained from the look-up table. The generation/consumption rate of water can be obtained by calculating the derivatives of the fluid volume variation which computes the difference between the fluid volume at current time step and the fluid volume of the previous time step divided by the current time step size. This value is cast into the two-phase transport model (i.e. Eq. (2)) as the source/sink term.

3. The quartz dissolution rate can be estimated as follows. The amount of dissolved SiO_2 for the current time step is updated by multiplying the quartz dissolution rate with the current time step size. The total accumulatively dissolved SiO_2 is thereby updated after each Newton iteration.

4. The porosity and pH values are updated for each Newton iteration.

5. The carbonation reaction is considered complete, as soon as chemical equilibrium is reached, i.e. the addition of additional CO_2 is not causing any more changes in mineral composition. ASR is considered complete once the quartz saturation index is close to 1 which indicates that the silica aggregate is in equilibrium with the overall chemical system. The specific threshold values for the completion of carbonation and ASR depend on the combination of reacted CO_2 and SiO_2 and are provided by the look-up table.

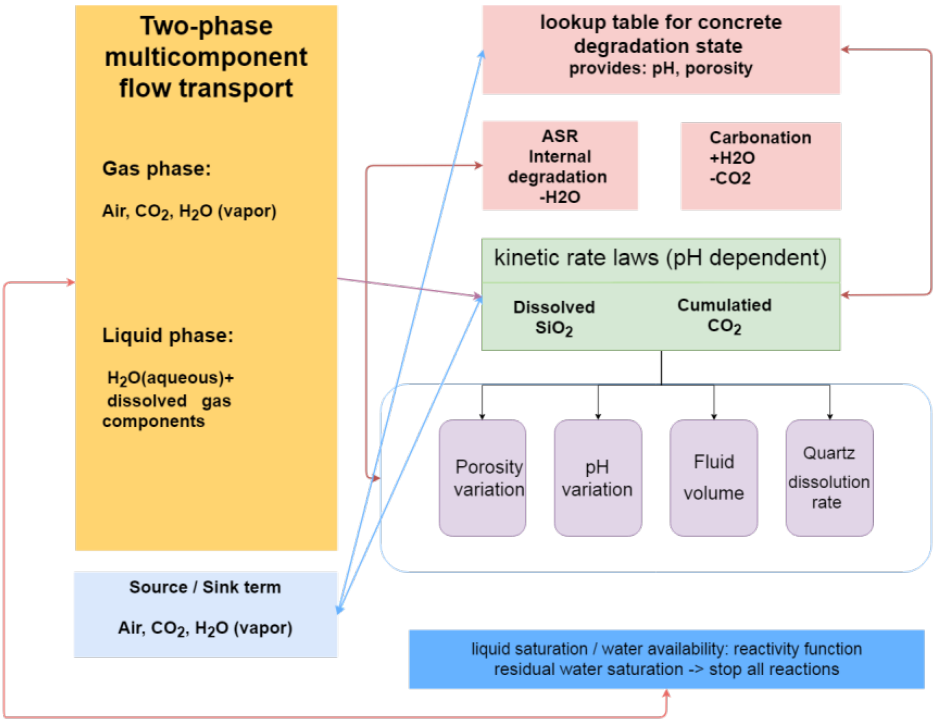


Figure 3: Schematic illustration of the coupling strategy between two-phase multi-component transport and chemical processes via the look-up table approach.

3 Validation of the look-up table approach

The pivotal question is how good and under which (transport) conditions the look-up table approach resembles the simulation results of a full reactive transport model. To tackle this question, we compared the newly developed code OpenGeoSys-MP-LT with the well-established reactive transport code OpenGeoSys-GEM (Kosakowski and Watanabe, [71]). A comprehensive comparison between both codes is hampered by the lack of multi-phase transport capability of OpenGeoSys-GEM which only supports transport in the liquid phase. It is not straightforward to extend the coupling to the multi-phase

solver implemented in OpenGeoSys V.5. Furthermore, it is important to note that OGS-MP-LT is based on OpenGeoSys V.6, a completely new implementation of OpenGeoSys V.5. OpenGeoSys V.6 lacks the reactive transport interface; therefore, it is also not possible to couple a GEM solver to OpenGeoSys-MP-LT.

Our intention is to show that we can replace the complex and costly chemical calculations by a pre-calculated look-up table for two specific cement degradation mechanisms and specific (multi-phase) transport scenarios. The two essential prerequisites in terms of transport and for the applicability of the look-up table are:

1) On continuum scale, the degradation of ASR does not require a macroscopic transport process. No macroscopic transport of dissolved silica in the liquid or gas phase is needed to drive ASR.
2) Carbonation is controlled by the transport in the gas phase. CO_2 fluxes in the gas phase are assumed to be many orders of magnitude higher than in liquid phase.

For these calculations, we assume that chemical reactivity is independent of the saturation state of the medium. At pore scale there is always a connected liquid phase that ensures very fast transport of reactants between quartz aggregates and cement phases.

Unfortunately, with the two employed codes, we cannot solve exactly the same multi-phase transport system. Still we can define a very simplified and to some degree even unphysical transport scenario for which both codes can approximate the dominant transport process and for which the differences become very small. We assume that diffusion of CO_2 in a gas phase is the only relevant transport mechanism in the gas phase. A system, for which CO_2 transport dominates the transport of all other reactive substance,

is a partially liquid saturated system, and CO_2 is the only reactive substance in the gas phase. In such a system, CO_2 diffusion is faster by 4 orders of magnitude in the gas phase than in the liquid phase [16], which allows for the separation of time scales for transport between (general) solute transport in liquid phase and CO_2 transport in the gas phase. Diffusive transport of dissolved CO_2 in the liquid phase can be considered. Both intrinsically include the effect of solubility of gases in water via Henry's law. The pore diffusion coefficient of gaseous CO_2 is assumed to be 1e-6 m^2/s while the pore diffusion coefficient of all aqueous species is 2e-10 m^2/s. This ensures that for the same gradients mass fluxes in the gas phase are 5000 times higher.

In addition, the benchmark scenarios were set up such that CO_2 concentrations in the gas phase were far beyond those at atmospheric conditions. This also increases the mass flux of CO_2 in gas phase. The liquid saturation state is assumed to be constant at 0.5 at every location throughout the course of the simulation. This effectively switches off the feedback of liquid volume changes during concrete degradation on multi-phase transport. This part of the look-up table cannot be benchmarked with the two codes. The effective diffusion coefficient in gas and liquid phase shall depend on changes of porosity via the following relation: $D_e = D_p \cdot 0.5 \cdot \phi(t)$, D_p is the pore diffusion coefficient in the gas phase. The relation allows a simple coupling between diffusive transport and porosity changes induced by mineral transformations.

OpenGeoSys-GEM does not include a coupling to the multi-phase transport modules of OpenGeoSys, but we were able to implement a simple transport process for diffusion of a single component in a virtual gas phase. This allows calculation of specific scenarios based on diffusion of CO_2 in partially saturated media without saturation change. A back-coupling of the effective diffusion coefficient on

porosity changes is implemented. Due to the inflexibility of interface between transport and chemistry it is not possible to switch off the transport of all dissolved species in OpenGeoSys-GEM. On the one hand, this allows the inclusion of diffusive transport of dissolved CO2 in the liquid phase, but it also allows the transport of other species which can potentially affect the progress of degradation front. In the general context of this benchmark, the thermodynamic setup used for look-up table creation was used and a constant temperature of 298.15 K and a pressure close to 105 Pa (1 Bar) was assumed for all calculations.

OpenGeoSys-MP-LT includes a complete multiphase multi-component transport module [72]. The gas phase is composed of CO_2, air and water vapor, but the air is assumed to have the same solubility as the CO_2 and does not participate in any reaction. At each time step, we calculate the total amount of CO_2 consumed by the carbonation reaction, then we compensate the system by adding the same amount of air into the system via the source term. This allows a "diffusion only" scenario in the system with no saturation and pressure variation. Ideal mixing of gas components is assumed over the simulation.

A subset of features was tested in the following benchmark which was limited to consider three cases, where case 3 was further split into of two sub-cases:

Case 0: Diffusive transport of CO_2 in the gas phase with and without consideration of gas solubility in liquid phase. No chemistry is taken into account in this case.

Case 1: Evolution of a concrete (pH, porosity) undergoing ASR only, and no relevant transport processes are considered. This benchmark tests essentially the implementation of the kinetic model for SiO_2 dissolution.

Case 2: Evolution of concrete (pH, porosity) undergoing accelerated carbonation (no ASR) where CO_2 diffusion in a gas phase is much faster than solute diffusion in a liquid phase.

Case 3: Evolution of partially saturated concrete (pH, porosity) undergoing accelerated carbonation and ASR. CO_2 transport is dominated by diffusion in a gas phase. Two sub-cases are considered:

Case 3a: CO_2 diffusion dominates, i.e. the progress of carbonation is much faster than the typical time scales for ASR. A 1D setup of a 1 m long concrete domain was applied here for the simulation.

Case 3b: CO_2 diffusion and ASR compete, i.e. part of the domain is highly affected by ASR before the carbonation front arrives. This case was implemented by enlarging the simulation domain by a factor of 10. In this setup the carbonation front needed 100 times more time until it reached the end of the simulation domain.

3.1 Model setup

- **Dimensions and discretization**

The default model setup was represented by a 1D concrete structure (length = 1m) using a regular mesh of 100 elements with node distances of 1 cm. Three variant cases were considered. The detailed set-ups for the benchmark case are summarized in Table 3.

Table 3: The dimensions, discretization and simulation time for each benchmark

	Process		**Domain**	**Domain discretization**		**Simulation**
	ASR	Carbonation	**scale [m]**	OGS-MP-LT	OGS-GEM	**time scale [year]**

Case0	×	×	10	100 elements	100 elements	10
Case1	√	×	1	100 elements	2 elements	10000
Case 2	×	√	1	100 elements	100 elements	30
Case 3a	√	√	1	100 elements	100 elements	30
Case 3b	√	√	10	100 elements	100 elements	2000

- **Transport setup**

In order to allow a comparison between OpenGeoSys-MP-LT and OpenGeoSys-GEM, the multi-phase transport process was simplified. A critical point in the benchmark cases was to constrain the setup for diffusion of CO_2 in the gas and liquid phases in such a way that both codes calculated the same diffusive fluxes.

CO_2 diffuses with an effective diffusion coefficient D_e that depends on the porosity, liquid saturation S and the free gas diffusion coefficient D_G = 1.0×10^{-6} m^2/s.

In OpenGeoSys-GEM the diffusion of CO_2 in the gas phase was implemented as an additional diffusion process in the completely liquid-filled porosity (S = 1) which otherwise did not interfere with “reactive” solute transport. In addition, only the “in-diffusion” boundary was open. The other boundary was closed with a zero-flux condition for liquid (no advective transport), solutes and CO_2.

In OpenGeoSys-MP-LT the pore space was split into two equal compartments by fixing liquid saturation to a value of 0.5. In order to reproduce the same D_e for CO_2 diffusion as in OpenGeoSys-GEM, D_G was increased by a factor of 2. Gas and liquid pressures were set to a fixed value at the “in-diffusion” boundary. The other boundary was closed in order to avoid advective fluxes in the column.

The density of all gases was set equal to the value of CO_2, thus avoiding induction of transport due to different gas densities and concentrations.

The thermodynamic and kinetic setup for the reactive transport calculations in OpenGeoSys-GEM were identical to the setup of the look-up table described before.

For diffusion the pore diffusion coefficient for solutes was set to 2.0e-10 m^2/s and for gases to 1.0e-6 m^2/s. The effective diffusion coefficient was calculated by multiplication of porosity and pore diffusion coefficient.

Automatic time step sizing was used for all simulations. In addition, the time step size was limited as listed in Table 4.

Table 4: Maximum time step sizes for simulation cases in OpenGeoSys-GEM and fixed time step sizes in OpenGeoSys-MP-LT.

	OpenGeoSys-GEM: Maximum time step size [s]	OpenGeoSys-MP-LT: Time step size [s]
Case 0	1e5(~3.169e-3 years)	1e5 (~3.169e-3 years)
Case 1	1e3 (~3.169e-5 years)	0-2500 yrs: 1.578e+5 (0.005 yrs) | >2500 yrs: 1.578e+7 (0.5 yrs)
Case 2	1e5 (~3.169e-3 years)	3.156e+4 (0.001 yrs)
Case 3a	1e3 (~3.169e-5 years)	3.156e+4 (0.001 yrs)
Case 3b	1e5 (~3.169e-3 years)	1.578e+5 (0.005 yrs)

The parameters specific for OpenGeoSys-MP-LT setup are listed in Table 5. For all simulations with OpenGeoSys-MP-LT fixed time step sizes are used (Table 4).

Table 5: Parameters for the simulation with OpenGeoSys-MP-LT.

Parameter	Symbol	Value	Unit
Intrinsic permeability	K	1e-19	m^2
Liquid phase viscosity	μ_L	1e-3	Pa · s
Gas phase viscosity	μ_G	9e-6	Pa · s
Molecular diffusion coefficient for gas component	D_G	2e-6	m^2/s
Molecular diffusion coefficient for liquid component	D_L	2e-10	m^2/s
Residual saturation for gas phase	S_{rG}	0	-
Residual saturation for liquid phase	S_{rL}	0.3	-
van Genuchten parameter	n	0.5	-
van Genuchten parameter	P_r	1e+6	Pa

- **Initial and boundary conditions**

The simulation domain is initially saturated with water and air. The initial water saturation was set to 0.5. Uniform temperature keeps at 25 °C. An atmospheric pressure was assumed over the whole domain. Initially, the gas pressure PG was 10^5 Pa, the capillary pressure PC was 3.35×10^6 Pa (corresponding to S_L = 0.5) and the molar fraction of CO_2 in gas was 0.001.

The boundary conditions are represented by a Dirichlet boundary with constant CO_2 concentration at the left point. The gas pressure at the boundary was 10^5 Pa, the capillary pressure was 3.35×10^6 (corresponding to S_L = 0.5) Pa and the molar fraction of CO_2 in gas was 0.999. A strongly CO_2 dominated gas phase with a concentration of 39.43 mol/m^3 (0.89e-3 kg/m^3) was assumed for the "in-diffusion" boundary of the column. Note that this value is much higher than the CO_2 concentration in the atmosphere which is close to 0.0158 mol/m^3 (385 ppm). Therefore, such a high CO_2 concentration gives rise to much faster carbonation than in atmospheric conditions (accelerated carbonation). The right boundary of the domain was closed with a with zero-flux boundary.

3.2 Results

- **Case 0 (Only transport)**

This benchmark aims at a comparison between two codes with only transport and no chemical reaction taken into account. Two variations are compared:

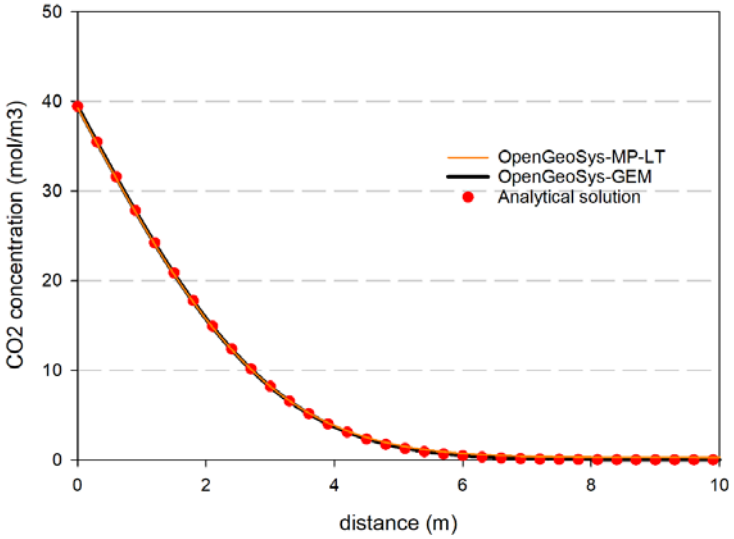
(a) The first case simulates the CO_2 transport in the gas phase without considering the solubility of CO_2 in the liquid phase.

(b) The second case takes the solubility into account.

Fig. 4 depicts the CO_2 transport front in the gas phase at the time = 0.09 year (2.84E+06 s) for case0-(a). An analytical solution is also presented for comparison. The analytical solution is given as:

$$c(x,t) = c_0[1 - \mathrm{erf}\left(\frac{x}{\sqrt{4Dt}}\right)] , \quad (13)$$

Where $c(x,t)$ corresponds to the CO_2 transport front, D is the diffusion coefficient. The detailed description of the analytical solution is given in B.J. Roth [73]. Good agreement can be observed between the OGS-MP-LT and OGS-GEMS. The results are also identical to the analytical solution.



595 **Figure 4: Gaseous CO_2 profiles at t=0.09 year for benchmark case 0-(a) with no CO_2 dissolution, and OpenGeoSys-GEM (black solid lines), OpenGeoSys-MP-LT (orange solid lines) and analytical solution (scatter points).**

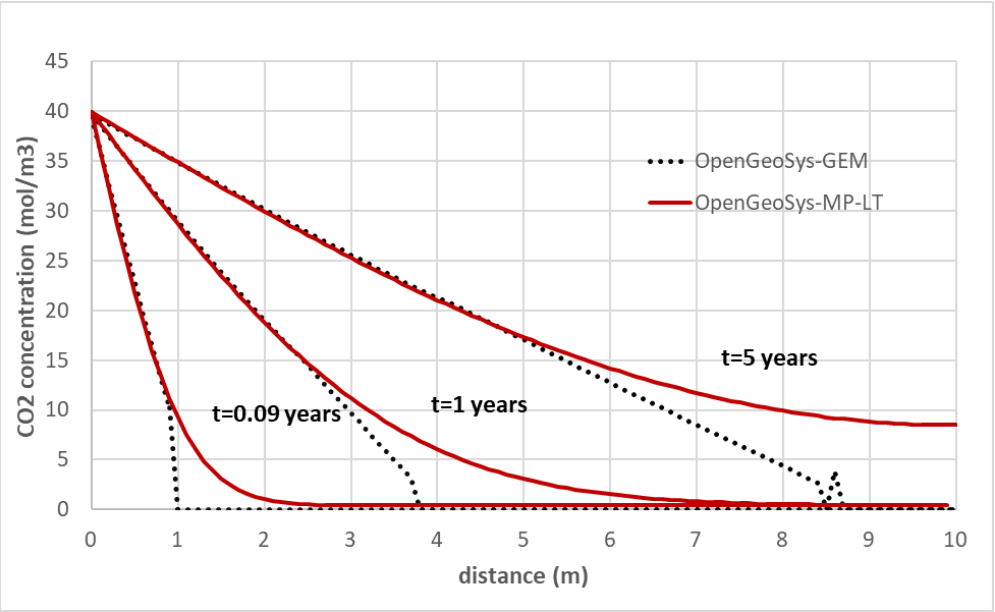


Figure 5: Gaseous CO_2 profiles at t=0.09, 1 and t years for benchmark case 0-(b) with CO_2 dissolution taken into account, and OpenGeoSys-GEM (black dashed lines), OpenGeoSys-MP-LT (red solid lines).

Fig. 5 presents the result of the second case of case 0-(b) which considers the solubility of CO_2. In general, the OpenGeoSys-MP-LT can produce identical CO_2 transport front to the OpenGeoSys-GEMS. However, there are differences between them when the CO_2 concentration is small.

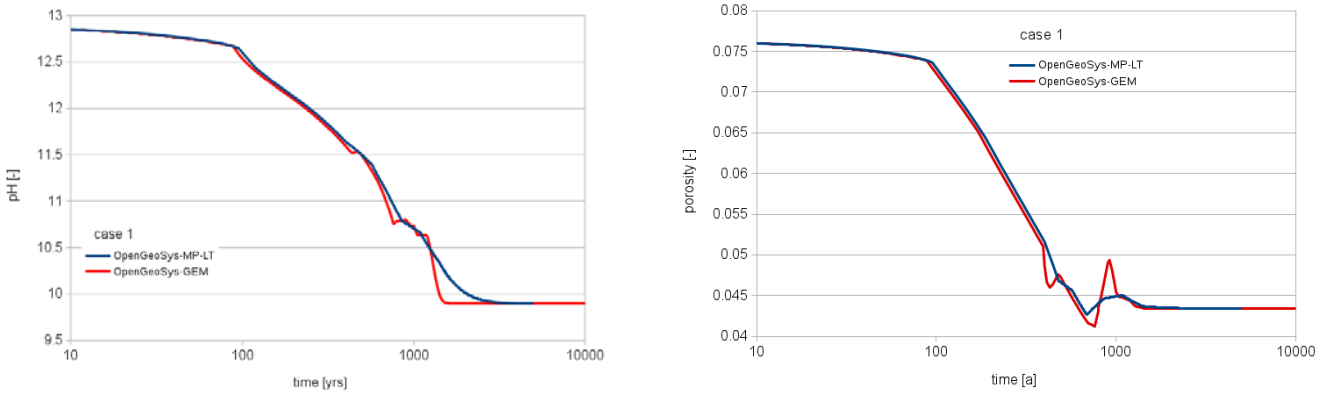
The difference can be attributed to the fact that in case of OGS-MP-LT, there is always a gas phase present, whereas with GEMS the gas phase is absent at the front (all CO_2 dissolved in liquid phase), and concentrations of CO_2 in the gas phase are set to zero.

In the case of reactive transport, such differences are smaller (as we can see in cases 2 and 3), because all the CO_2 in liquid phase is consumed by reactions and the smeared diffusive front for OGS-MP-LT is not present. This difference in transport/chemistry coupling does influence the fronts a bit, but obviously not too much.

- **Case 1 (ASR only)**

Case 1 essentially corresponds to batch calculations as for both codes, OpenGeoSys-MP-LT and OpenGeoSys-GEM, the evolution at all finite element (FE) nodes is identical. This was achieved by not applying special boundary conditions which suppress concentration gradients and transport in gas and liquid phase.

The first FE node at the left-hand side boundary was selected to plot the temporal evolution of the pH value and porosity (Fig. 6).



(a) pH value evolution

(b) porosity evolution

Figure 6: The temporal evolution of pH value (a) and porosity (b).

The blue lines represent results generated by OpenGeoSys-MP-LT, while the red curves denote the OpenGeoSys-GEM results. The results demonstrate a very good agreement between the two codes. The fully reactive transport model shows additional variations in pH and porosity with time at around 800-

1000 years. These variations are not covered by the look-up table, as they are related to increments in SiO_2 which are smaller than the resolution of the look-up table (ΔSiO_2 = 0.2 mol/l).

Fig. 7 shows the evolution of the batch reaction system in terms of time-dependent mineral volumes calculated by the OpenGeoSys-GEM code. To highlight the minerals with active changes, calcite, quartz, inert phases and some part of C-S-H that make up 80 % of the volume are not shown in this figure. The cement phases are transformed in the same sequence as shown in Fig. 1. The use of the kinetic rates for aggregate dissolution relates the SiO_2 amounts with a time scale. For this setup portlandite is dissolved after 85 years, hydrogarnet after 380 years, ettringite after 855 years, hydrotalcite after 1075 years and thermodynamic equilibrium is reached after about 1600 years.

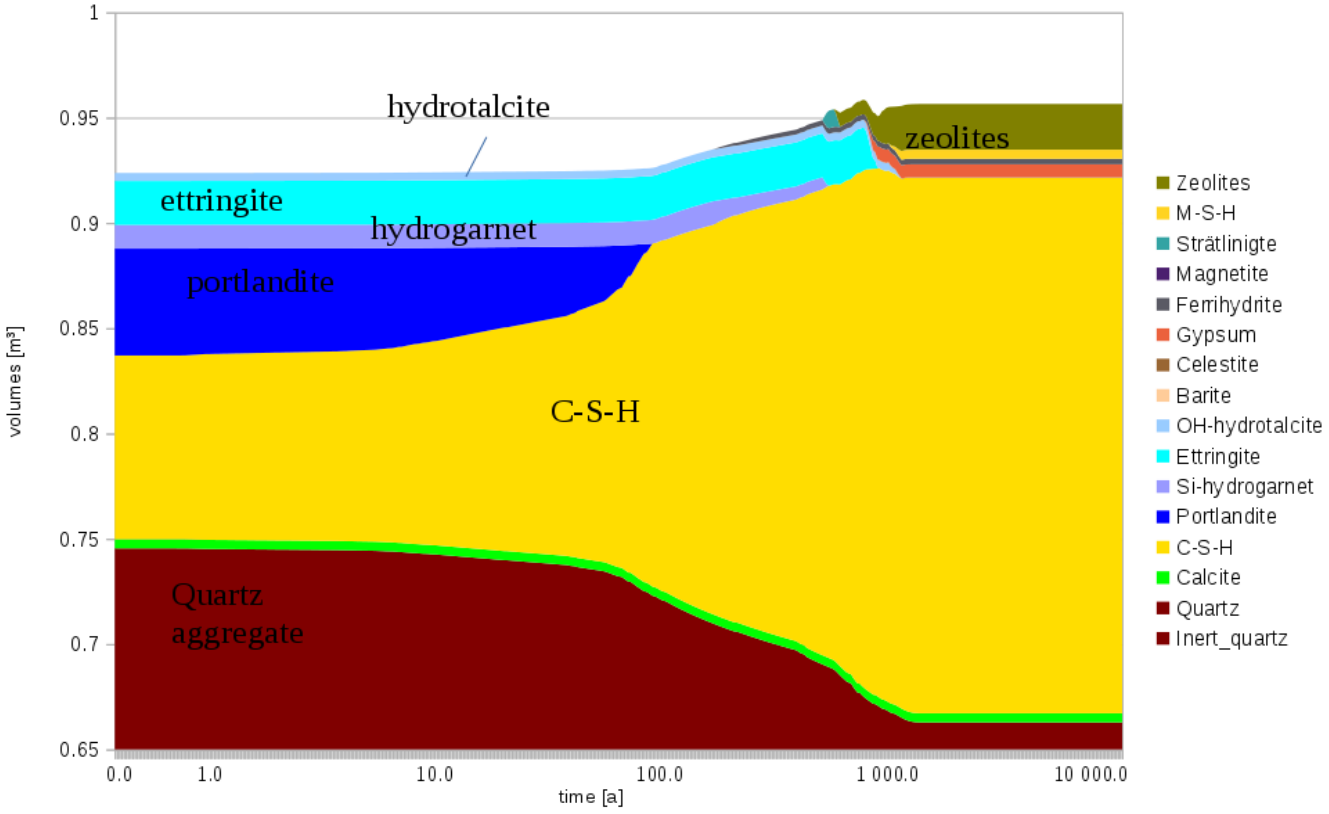


Figure 7: Mineralogical evolution with time shown as volume fractions. The porosity corresponds to 1 (sum of solid volume fractions). Calcite, quartz, inert phases and some part of C-S-H that make up 80 % of the volume are not shown.

- **Case 2 (Carbonation only)**

The benchmark case 2 was designed to check applicability of the look-up table approach for the case of carbonation only. Fig. 8 shows spatial profiles for CO_2 concentrations in the gas phase at different times. The pH and porosity profiles at the same times are shown in Fig. 9. Agreement between both approaches is relatively good, although after 10 to 20 years the reactive transport approach predicts faster progress of the carbonation front compared to the look-up table approach. It should be noted that the progress of the carbonation front is dependent on the square root of time which is typical for reactive fronts driven by diffusive transport.

The pH profiles show some overshooting by OpenGeoSys-GEM at the onset of the carbonation front which coincides with a stronger interim reduction of the porosity. The porosity reduction is caused by the interim formation of zeolite (chabazite), which occurs when portlandite dissolution is completed and ettringite is dissolved (Fig. 10). Chabazite, which is a hydrated calcium aluminum silicate, takes up considerable amounts of H_2O from the pore water. Removal of H_2O from the pore water increases the alkali concentrations and consequently pH. Due to the small stability field of chabazite, this effect is not covered by the look-up table and therefore not reproduced by OpenGeoSys-MP-LT. The mineralogical profile in Fig. 10 shows that most mineral transformations follow a step function, except for the dissolution of portlandite. Note that the direction of transport is from left to right, i.e. the completely degraded concrete is on the left and intact concrete is on the right side. The smoothed dissolution profile

indicates some effect of numerical diffusion related to the steep concentration gradients for CO_2 in the gas phase and all solutes in liquid phase near the carbonation front. This numerical diffusion might be also responsible for the faster progress of the carbonation front as indicated by the OpenGeoSys-GEM results.

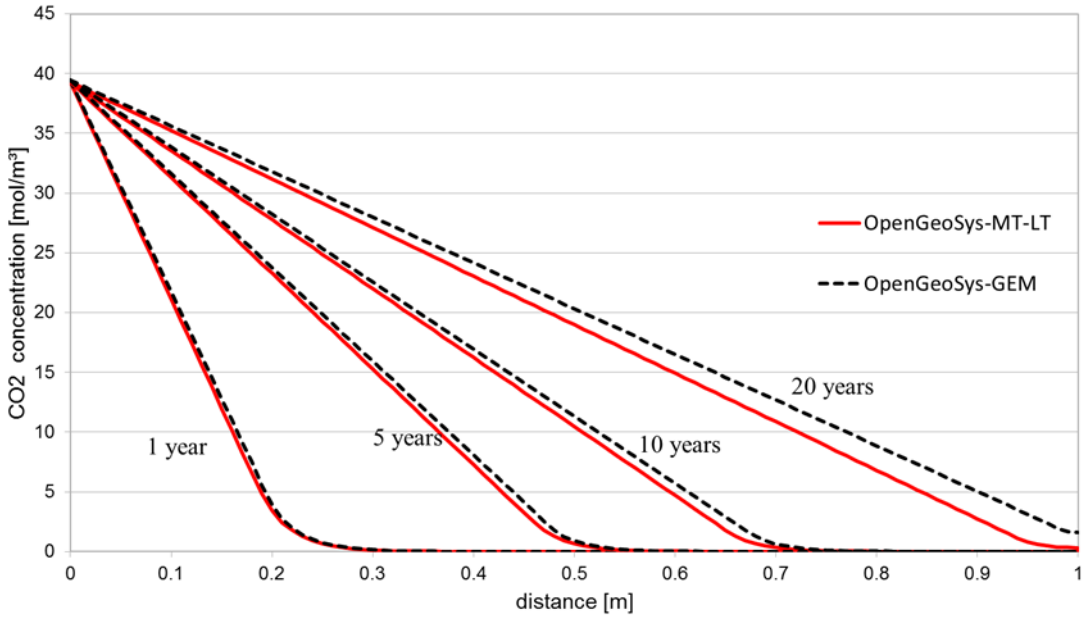


Figure 8: Gaseous CO_2 profiles at different times for benchmark case 2 and OpenGeoSys-GEM (black dashed lines) and OpenGeoSys-MP-LT (red solid lines).

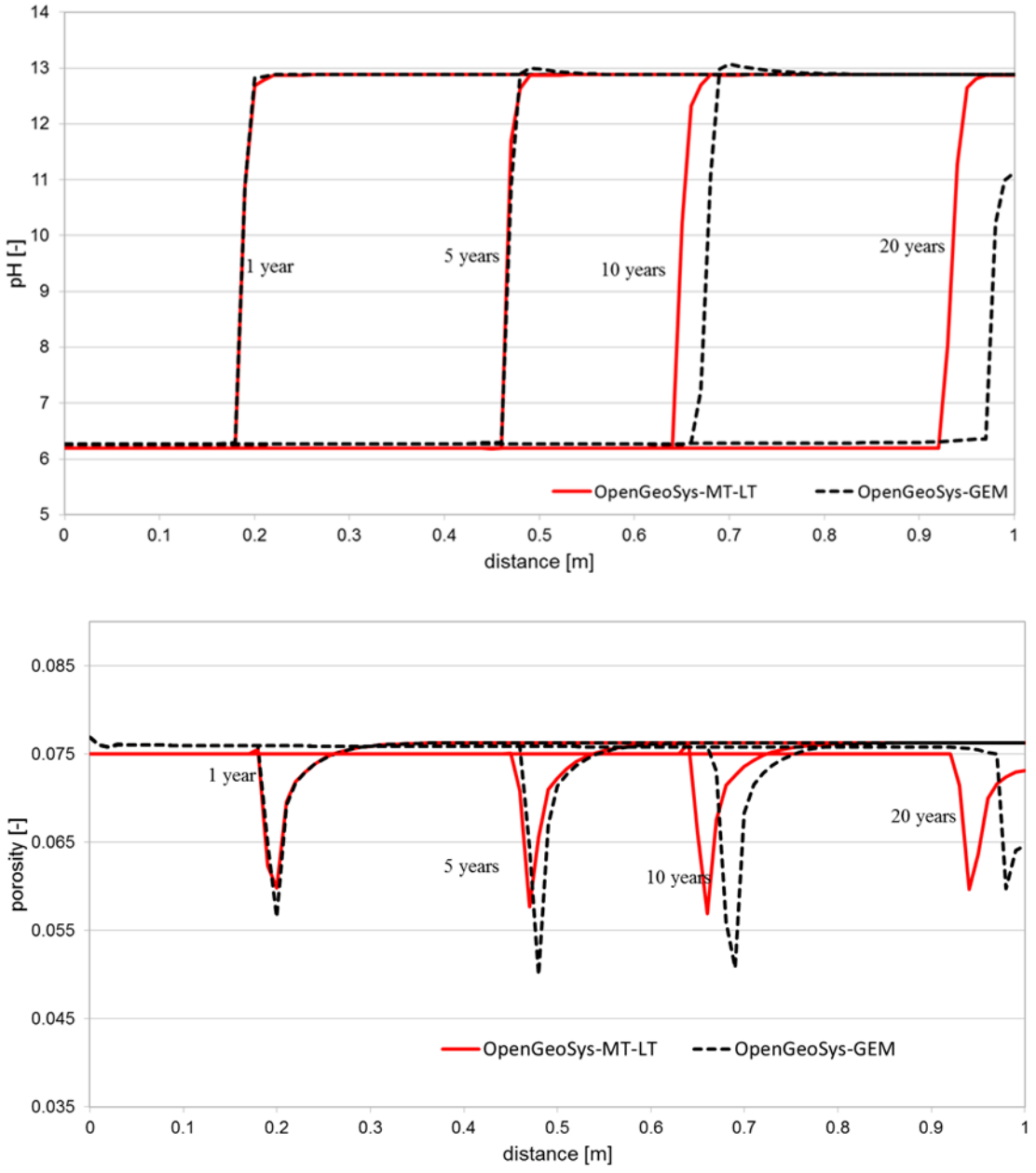


Figure 9: Simulated pH and porosity profiles at different times in benchmark case 2 and OpenGeoSys-GEM (black dashed lines) and OpenGeoSys-MP-LT (red solid lines).

665

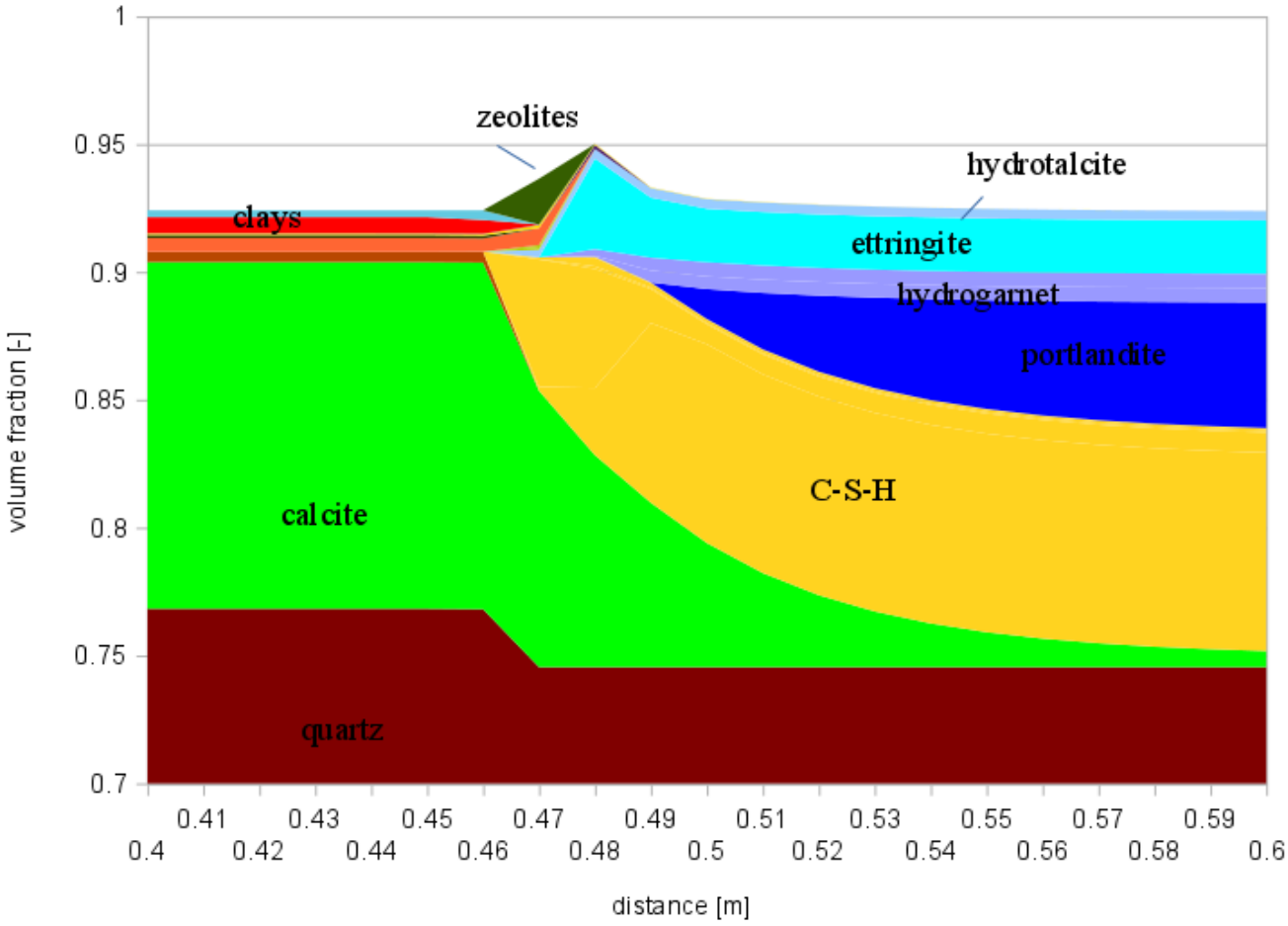


Figure 10: Mineralogical profile after 5 years of simulation time produced by OpenGeoSys-GEM.

- **Case 3a (fast carbonation and ASR)**

Case 3a compares the combined effect of carbonation and ASR over a relatively short distance, i.e. in this case concrete degradation due to carbonation is dominant. The system evolution is therefore expected to be very close to case 2. Comparison of the profiles for gaseous CO_2 (Fig. 11), pH (Fig. 12) and porosity (Fig. 13) resemble the corresponding profiles of case 2 (Fig. 8 and Fig. 9) very much.

The advancement of the carbonation front is a little bit faster than the one predicted in case 2. Within 20 years, ASR consumes already a portion of the portlandite which reduces slightly the amount of CO_2 necessary to complete carbonation. For the fully reactive transport model, after 1 m, the carbonation front has already passed the model boundary, and it is out of the view. Therefore, the front at time t = 19.65 years is plotted for comparison with the look-up table approach. As previously mentioned in connection with case 2, the faster progress of the carbonation front can be explained by an enhanced numerical diffusion in the OpenGeoSys-GEM code.

In the porosity profiles (Fig. 13) some oscillations are visible for the OGS-GEM results on the left side, i.e. behind (left of) the carbonation front. These oscillations are induced by numerical oscillations in the transport solver caused by strong temporal variations in the concentrations near the carbonation front. Concentration oscillations are smoothed at the expense of small mineralogical changes as the chemical solver enforces equilibrium between pore water composition and mineralogy. In the specific setup for concrete carbonation it is believed that the solid solution model for C-S-H phase reacts particularly sensitively to changes in the pore water composition. The concentration oscillations from the transport solver are not random. They occur at the same position relative to the carbonation front. The carbonation front moves slowly or even might stay at the same position over a long period of time, which causes an accumulation of mineralogical changes over many time steps.

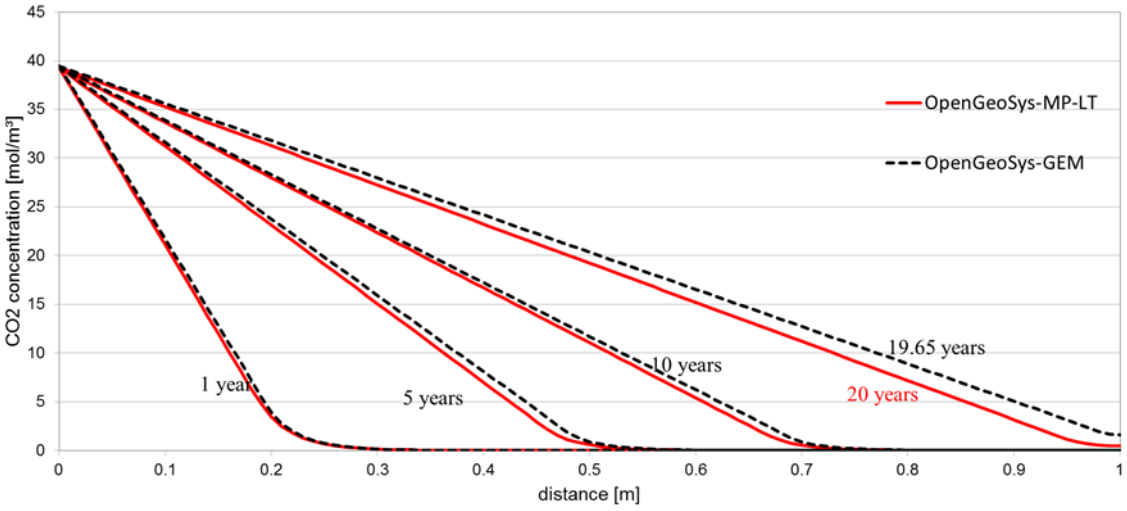
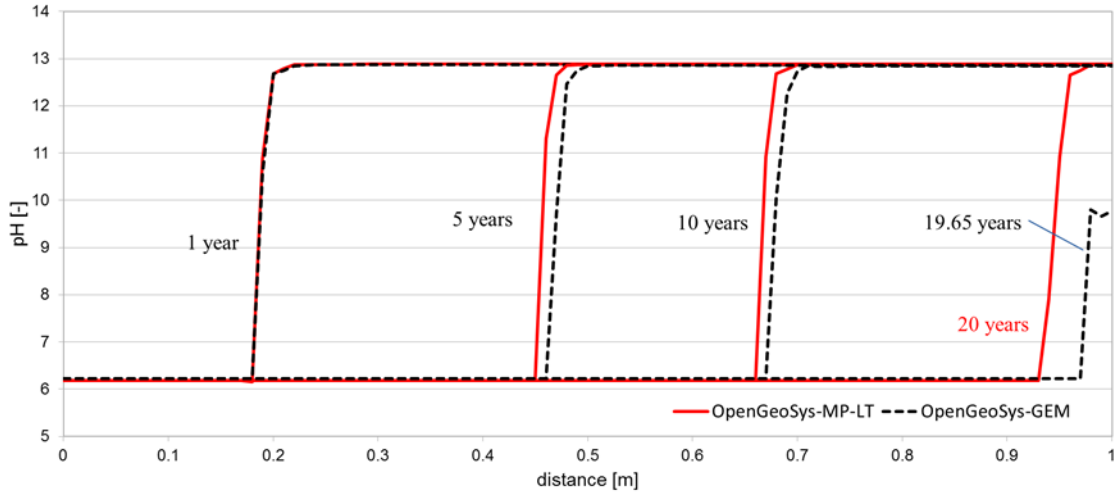


Figure 11: Simulated gaseous CO_2 concentration profiles at different times in benchmark case 3a. The right side of the simulation domain at 1 m is a closed boundary.



695 **Figure 12: Simulated pH profiles at different times in benchmark case 3a. The right side of the simulation domain at 1 m is a closed boundary.**

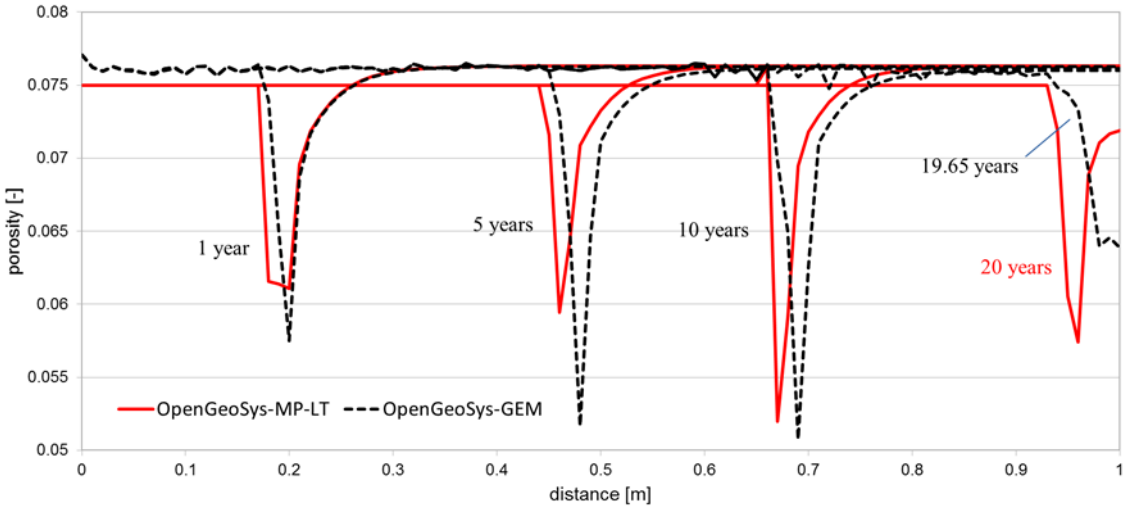


Figure 13: Simulated porosity profiles at different times in benchmark case 3a. The right side of the simulation domain at 1 m is a closed boundary.

- **Case 3b (carbonation and ASR)**

Case 3b extends case 3a to the full competition between carbonation and ASR. On the left side of the domain, at early times, carbonation dominates, whereas on the right side, ASR is the only process degrading the concrete. This case is a simple extension of case 3a in terms of a 10-times longer simulation domain. This was achieved by simply increasing the FE node distance 10-fold. As for case 3a on the left side (x=0 m) the CO_2 concentration in the gas phase was fixed, whereas the right side of the domain was closed, i.e. a no-flow boundary was applied on both the gas and liquid phase. As the progress of the diffusion-driven carbonation front follows a relationship which depends on the square root of time [16], it would take the carbonation front – in the absence of ASR – about 2000 years to reach the right boundary. This is 100 times longer than the time obtained in case 3a (~ 20 years). From

710 the calculations performed in connection with case 1 it is clear that the ASR is mostly completed within 2000 years.

Results of the calculations are given in terms of CO_2 concentration in the gas phase (Fig. 14), pH profiles (Fig. 15) and porosity profiles (Fig. 16). In general, the same effects for case 3a can be observed in this case, while they are superimposed by the ASR. As a consistency check, the carbonation
715 front progress after 10 years in the cases 3a and 3b is the same, although discretization and time step size were different. This shows that the difference between the look-up table approach and full reactive transport is also similar. In the cases 2 and 3a the carbonation front propagates slightly faster for reactive transport calculations than with the look-up table approach. In addition, variations of pH, mineral transformations and porosity near the carbonation front become stronger with time. With time,
720 diffusive transport of solutes other than CO_2 increasingly influences concrete carbonation. The effect of chemical gradients across the carbonation front becomes more important with time. Over time, CO_2 gradients and fluxes become smaller and the progress of the reaction front decelerates correspondingly. This behavior is described by the well-known square root relation ($x \sim \sqrt{t \cdot D_a}$) [11] where D_a is an apparent diffusion coefficient which includes the retardation due to chemical reactions. The slow-down
725 of the front allows geochemical differences across the carbonation front to be equilibrated over longer time steps. The influence of chemical gradients other than CO_2 (in gas and liquid phase) is not covered by the look-up table approach. ASR does not depend on continuum-scale spatial gradients in the look-up table; it is implemented as an internal source term for SiO_2.

Interestingly, small differences in the progress of ASR are more evident from the porosity changes over
730 time than pH evolution. The pH changes with time in a more stepwise way, whereas porosity oscillates

more strongly at intermediate pH values due to formation of intermediate phases (compare Sect. 3.2.1, Fig. 6 and Fig. 7).

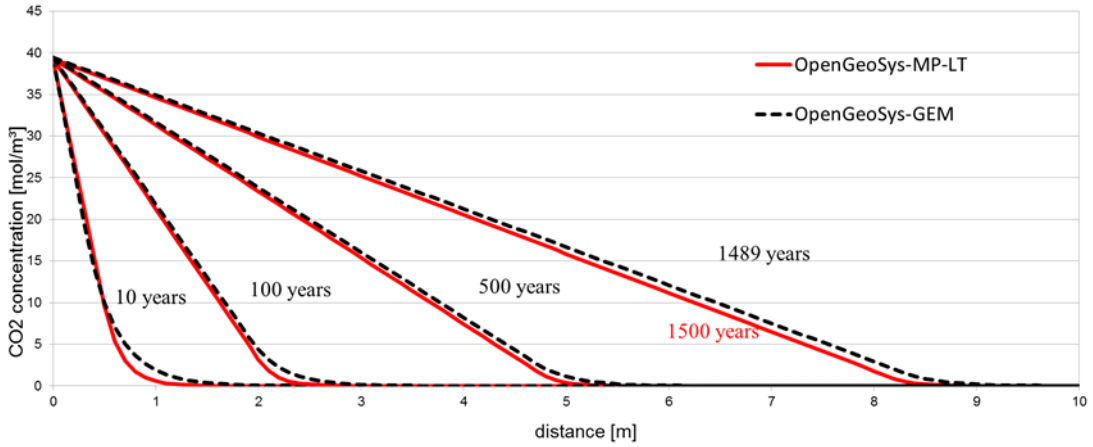
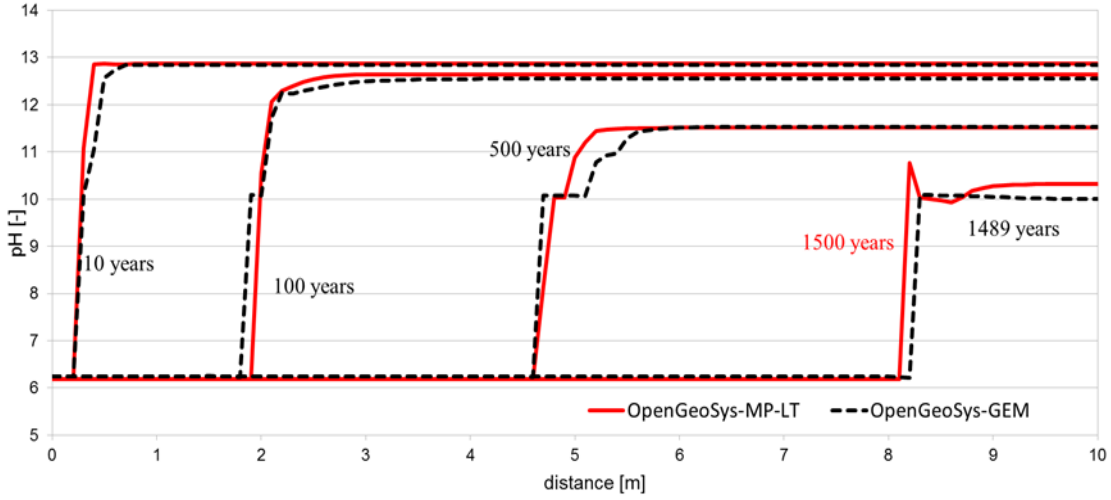


Figure 14: Gaseous CO_2 concentration profiles at different times for benchmark case 3b.



735

Figure 15: pH evolution profiles at different times for benchmark case 3b.

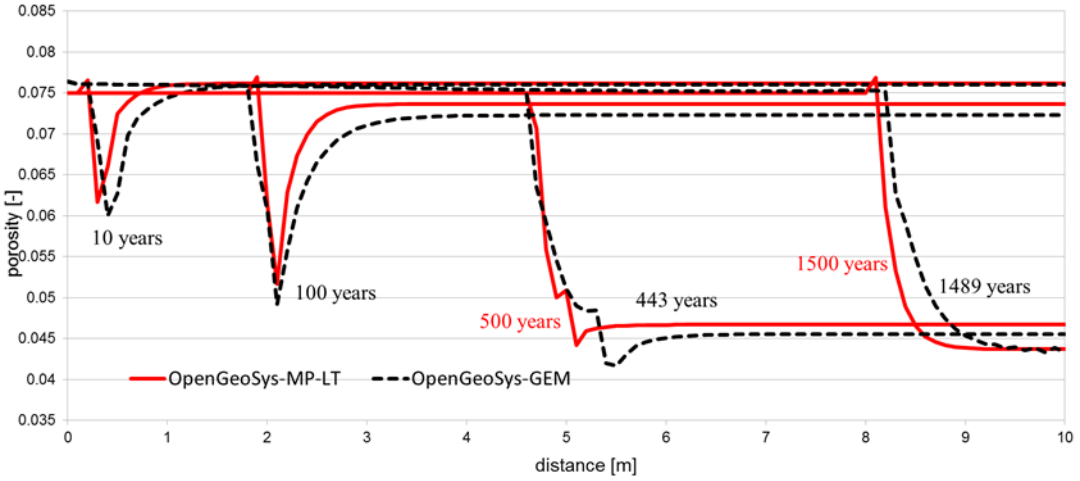


Figure 16: Porosity profiles at different times for benchmark case 3b.

- **Effects of the resolution of the look-up table**

In order to study how the different resolution of the look-up table affect the performance of the look-up table-based approach, we create a refined look-up table with a factor of ~16 higher resolution compared to the previous one, i.e. the entries in the look-up table is calculated from 0 to 4 mol with a step size of 0.05 mol for SiO_2 and CO_2 instead of 0.2 mol. Therefore, the refined look-up table is composed of 6400 sampling points. The newly created table is applied to simulate the benchmark case 3b.

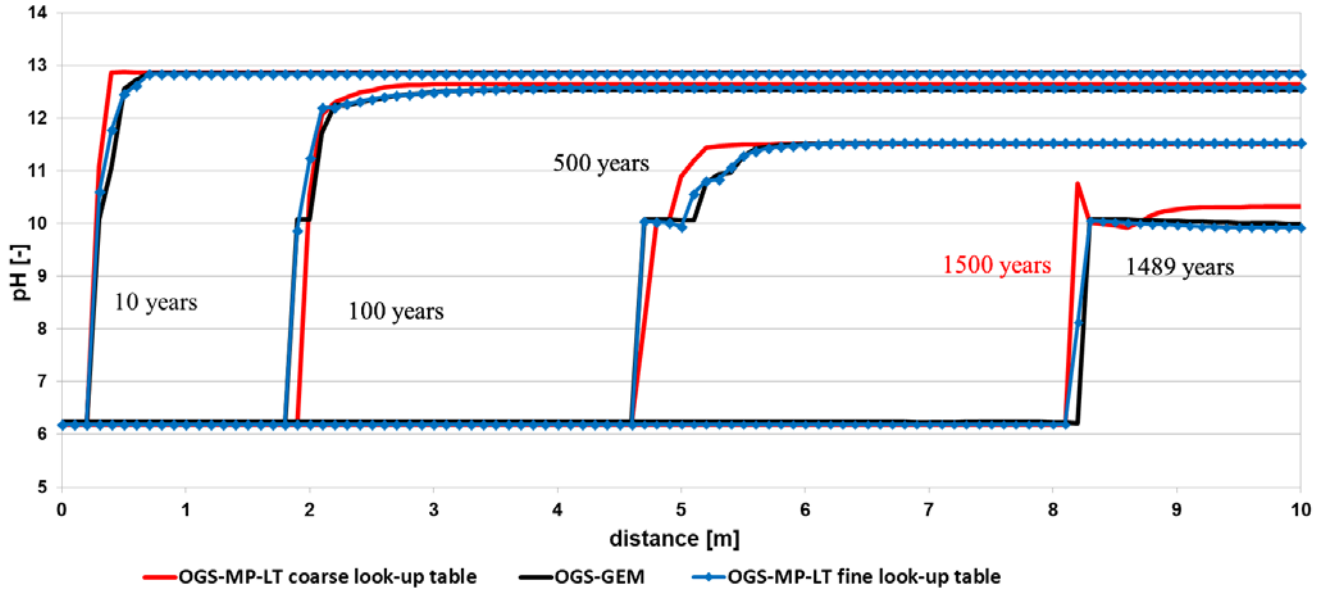


Figure 17: pH profiles at different times for benchmark case 3b with a finer resolution look-up table.

750

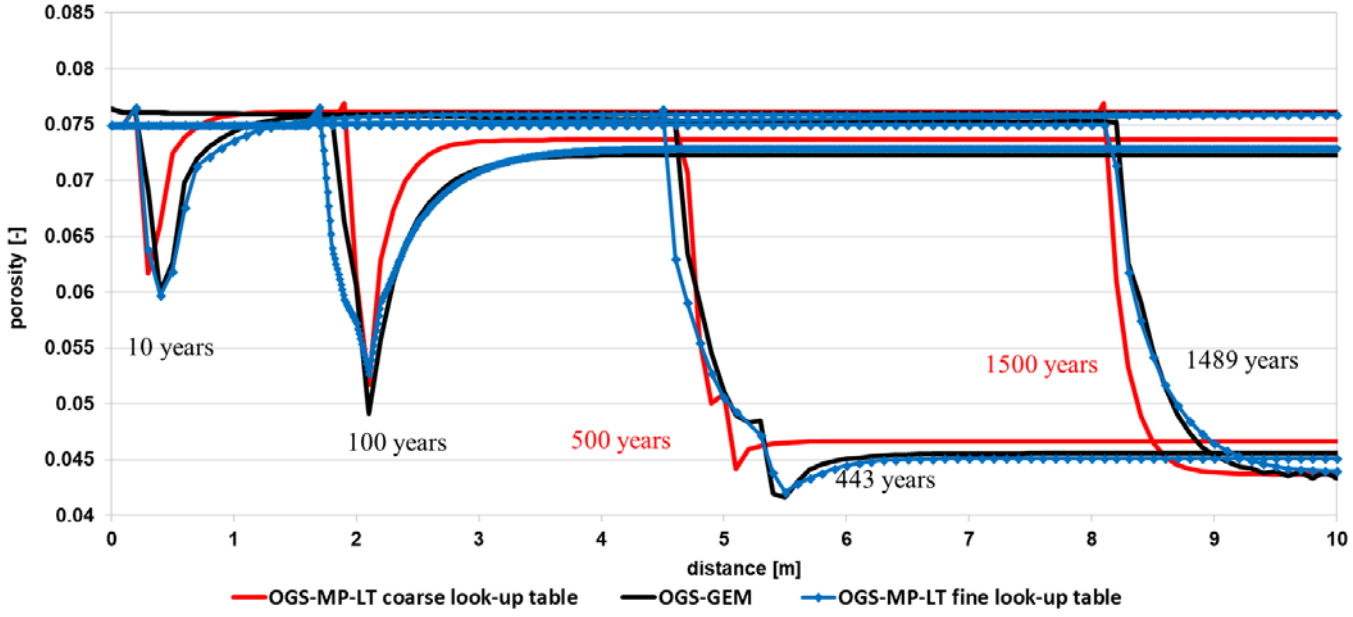


Figure 18: Porosity profiles at different times for benchmark case 3b with a finer resolution look-up table.

Fig. 17 and 18 depict the profile of pH and porosity at different times with the higher resolution look-up table. It can be clearly observed that by increasing the resolution of the look-up table, a significantly better match with the full reactive transport code OGS-GEM can be achieved.

The accuracy of the look-up table significantly depends on the resolution of the sampling data of the tables. Therefore, refining the data grid in order to improve the accuracy of the interpolations in the look-up tables is efficient and yield sufficiently accurate interpolated data.

- **Computational efficiency**

Besides the accuracy of the simulation results, the computational efficiency of the look-up table approach is of major interest which can be a crucial point especially for large-scale problems. We summarize the computational time required by both codes to calculate 400 time steps of the benchmark case 3b in Table 6. All the computations are conducted on a workstation with two Xeon E5450 quad-core CPU running Linux as the operating system. The two codes were compiled with GCC version 8.1.1 with optimization –O3 for OpenGeoSys-MP-LT and –O2 for OpenGeoSys-GEM. From internal measurements of CPU time in OpenGeoSys-GEM we know that for this system about 95% of CPU time is spent for solving the chemical system at each FE node for each time step. OpenGeoSys-GEM uses multi-threading for parallel chemical calculations and can utilize the 8 hardware threads of the workstation. Sixteen threads are used in order to achieve better load balancing between the threads, as full chemical calculations might need very different calculation times. For this example, a speedup of ~ 6.5 was observed for OpenGeoSys-GEM using 16 threads instead of 1 thread for chemical calculations.

Table 6: Computational times for calculation of 400 time steps of the case 3b benchmark case. Measured values are rounded to full seconds or two digits.

Time	Computational time[s]			
	OpenGeoSys-GEM (16 threads for chemical calculations)	OpenGeoSys-GEM (1 thread for chemical calculations)	OGS-MP-LT (NO Parallelization)	OGS-MP-LT (NO Parallelization, high resolution)
real time	115 s	748 s	8.2 s	8.7 s
CPU (user) time	742 s	743 s	7.9 s	8.9 s
system time	0.51 s	0.36 s	0.51 s	0.42 s

Table 6 compares performance of the different codes measured in a simple way with the Linux "time" command. The "real time" is the elapsed time needed for execution of the benchmark, CPU time is the cumulated time on all CPU that the process spent in user mode, and the "system time" is the time that the process spent in kernel mode. One should note that the time needed to solve the transport calculations in the two codes is not directly comparable, as different transport equations are solved.

The look-up table-based approach OGS-MP-LT with no parallelization leads to a factor of ~90 times speedup compared to the non- parallelized OpenGeoSys-GEM. While for the parallelized OpenGeoSys-GEM with 16 threads, the speedup can be achieved by a factor of ~14. The speedup in terms of CPU

time is the essential value, as the faster execution of multi-threaded OpenmGeoSys-GEM can be only achieved on specific hardware utilizing more CPU resources.

In order to gain some insight into the computation efficiency with different resolutions of the look-up table, we further include the computational time of the high-resolution look-up table in Table 6. It can be clearly observed that by increasing look-up table size up to a factor of ~16 times, the computational time is only increased by less than 10 %. Therefore, increasing the sampling points and using a high-resolution table have only limited influence on the computation efficiency.

4 Discussion

From the benchmarking exercise, two main factors have been identified to cause differences between the look-up table approach and full reactive transport.

1) The accuracy of the look-up table has very high sensitivity to the resolution of the sampling data in the table. The resolution of the look-up table used for the benchmarks does not cover all variations in porosity, pH or quartz dissolution rates in detail. This is obvious from the temporal evolution of pH and porosity associated with ASR as shown in Fig. 6. The accuracy of the look-up table approach can be improved by including interpolation points for maxima/minima of porosity/pH/rates and/or by covering regions with strong changes with a finer mesh of sampling data points. This is demonstrated in Fig. 17 and 18.

As previously mentioned, the look-up table approach does not cover the entire variability of the chemical system. Variability of the parameters below the sampling scale is smoothed out due to the

bilinear interpolation scheme. The absolute minimum porosity for carbonation might not be included in the look-up table as it is reached only for a very narrow intermediate stage of carbonation.

The progress of the carbonation front is a direct function of the diffusive CO_2 flux. From Fick's law it is clear that for a given CO_2 concentration gradient the flux is controlled by the effective CO_2 (gas) diffusion coefficient. In our simplified setup effective diffusion coefficient is calculated as the product of porosity and pore diffusion coefficient. A mismatch in the porosity evolution upon concrete degradation should influence the diffusion of CO_2 and might affect the progress of carbonation fronts. The interpretation of the porosity profiles in Fig. 9, Fig. 13 and Fig. 16 is not straightforward, as absolute porosity minima with time are not necessarily present within the plotted time steps. It seems that OpenGeoSys-GEM systematically calculates a slightly bigger intermediate porosity reduction. These values might be even smaller than those calculated with the look-up table as the diffusive transport of reactive species other than CO_2 in the aqueous phase influences transformation of mineral phases. Nevertheless, lower porosity values should reduce diffusive fluxes and slow down the progress of the carbonation front. Note that the opposite was observed which shows that other processes have a bigger influence on the observed diffusive fluxes.

2) Reactive transport calculations with OpenGeoSys-GEM are extremely sensitive to numerical oscillations in the solution of the transport equations. With the standard Galerkin FE methods, as used in OpenGeoSys, undershooting and overshooting of the solution are a common problem at reaction fronts with steep concentration gradients. Often numerical oscillations are quite strong and spread out into the whole calculation's domain.

As the magnitude of these oscillations is different for each transport equation, the chemical system may become poorly defined, and the GEM algorithm fails to reach a solution. We observed this problem at nearly all nodes in several benchmark runs. There are some methods available in OpenGeoSys which enable to suppress the numerical oscillations. For example, for some systems a flux-corrected transport (FCT) method was successfully applied [49]. For the current benchmark calculations “mass lumping” was used. The drawback of this method, like FCT, is that it causes an additional diffusive flux (numerical diffusion) in the transport equations causing reaction fronts to proceed faster.

It is shown from the above benchmark study that in both codes the time step size has to be small in order to properly approximate the progress of the carbonation front. Time step size Δt depends on the Neumann stability condition [74], which in turn depends on the spatial discretization Δx (FE node distance). With a very refined discretization, the time step size may become a computationally limiting factor.

One way to overcome limitations in time step size for OpenGeoSys-MP-LT is to use source/sink terms derived from the look-up table in a fully implicit way instead of an operator-splitting approach to include the look-up table. The fully implicit method allows achieving improved numerical stability and enabling a larger time step size. This further allows an automatic time stepping regime to be included with time step size not limited by the Neumann stability condition, but rather by changes in the reaction rates (e.g. completion of carbonation at a node).

The results of our study demonstrate that the use of a look-up table for concrete degradation is a good substitute for a chemical solver, for situations where chemical reactions happen locally and are either controlled by very slow reaction kinetics (quartz dissolution) or by external mass fluxes (CO_2 transport).

By “locally” we mean that we can clearly separate time and length scales between chemical and transport processes. The look-up table approach assumes that the progress of reaction is driven by some external kinetic or transport process. There are observations (e.g. Thiery et al. 2007[16]) that highlight the importance of reaction kinetics for carbonation. They show that carbonation fronts are not step functions and that cement phases do not necessarily react in a sequential way (as it is typical for equilibrium reactions reactions). If transport processes (for CO_2) are too fast compared to the kinetically controlled carbonation reactions (for different cement phases) the assumption of local equilibrium (chemistry) is not applicable. In situations where degradation process is heavily influenced by simultaneous reaction of several internally (kinetically) controlled reactions, the applicability of the look-up table is questionable. For example, it is neither possible to describe the exact shape of a carbonation front on small scale with the current look-up table approach, nor with a reactive transport model that does not include kinetic control of dissolution/precipitation of mineral phases.

The local chemical reactivity might be also influenced by other external processes or averaged material properties. On sub-continuum or pore scale, ASR requires the transport of reactants between aggregate grains and cement phases. This actually means that there has to be a liquid phase in order to allow the dissolution of reactants and there needs to be a connected pathway. The extent of such connected pathways on pore scale is heavily dependent on the pore size distribution and on the saturation state. Typically, the connectivity of the liquid phase decreases with saturation, and below some threshold saturation only isolated pores are liquid-filled. This type of relation between saturation and sub-continuum scale control of chemical reactivity can be expressed for example in form of a reactivity function, similar to the function used by Bǎzant and Najjar [75] for cement hydration. This approach is

already successfully employed by P. Thouvenot et al. [76] in reactive transport models for scaling the general chemical reactivity with saturation of concrete. It should be noted that it in principle would be required to introduce different reactivity functions for different processes (ASR or carbonation) and different mineral phases.

5 Conclusions and outlook

In this study, a new, coupled two-phase reactive transport model derived from the look-up table approach has been presented to simulate the long-term degradation of concrete due to ASR and carbonation. The proposed model is validated by the means of comparison with a full reactive transport model. In general, the proposed approach shows the same system evolution as the reactive transport models. Differences in the propagation speed of carbonation fronts are not necessarily related to the approach itself and can be attributed to numerical diffusion.

In terms of calculation time, it was observed that the serial (not parallelized) version of OpenGeoSys-MP-LT leads to a factor of ~14 faster than OpenGeoSys-GEM which employs 16 threads for chemical calculations. The approach presented in this study leads to a significant reduction in computational efforts, while maintaining numerical stability and good accuracy.

The accuracy of the look-up table approach can be further improved by including interpolation points for maxima/minima of porosity/pH/rates and/or by covering regions with strong changes with a finer mesh of interpolation points. Depending on the way the look-up table is used in the multi-phase multi-component transport codes this might cause problems. With OpenGeoSys-MP-LT the possibility was

tested to include the look-up table in terms of rates also for porosity changes. These rates (time derivative of porosity) may strongly vary between interpolation points which could cause convergence problems in case of the non-linear equation solver. For example, the variability of porosity very much depends on the choice and quality of thermodynamic data for clay and zeolite minerals.

The look-up table approach can be applied to problems where the transport of CO_2 – preferably in the gas phase – is much faster than the transport of other reactive solutes in the liquid phase. There are scenarios in the framework of radioactive waste disposal where macroscopic transport of dissolved silica might influence the long-term performance of the engineered system of a radioactive waste repository [see e.g. ,77]. These scenarios are related to skin formation and porosity clogging at clay/cement interfaces with a distinct dependency of clogging time on numerical discretization and kinetic parametrization [78]. Given the very small extent of the influenced volume and the complexity of porosity clogging [79], an approximation of the localized change of transport properties by time-dependent functions seems more appropriate.

Furthermore, the formation and transformations of zeolite and clay minerals at later stages of concrete degradation are kinetically controlled. Here, an additional multiplicative function for the accounting of a kinetic slowdown of reactivity needs to be introduced, similar to the function used by Bažant and Najjar [80] for cement hydration.

As the future topic of the work, the improved computational efficiency of the chemical reaction part makes the proposed model particularly promising in further coupled with the geomechanical model in OpenGeoSys [81] for a multi-scale and multi-chemo-physics analysis of the evolution of the concrete.

Declarations

List of abbreviations

AAR: Alkali-aggregate reaction

ACR: Alkali-carbonate reaction

ASR: Alkali-silica reaction

C-S-H: Calcium-silicate hydrates

FCT: Flux-corrected transport method

FE: Finite element

L/ILW: Low/intermediate level waste

M-S-H: Magnesium silicate hydrates

PDE: Partial differential equation

OGS: OpenGeoSys

OpenGeoSys-MP-LT: OpenGeoSys multiphase transport module with a look-up table approach

Ethics approval and consent to participate

Not applicable

Consent for publication

Not applicable

Availability of data and material

The OpenGeoSys (V.6) is freely available to use. The source code can be accessed by following the instruction at: http://www.opengeosys.org/. As indicated in the text, a modified version OpenGeoSys-MP-LT is used in this work, which can be freely acquired via the link: https://github.com/Yonghui56/ogs/tree/carbonation_ncomp_altern.

The version of OpenGeoSys-GEM modified for work is available from http://github.com/kosakowski/OGS5GEMDEV.git. The repository also includes the input files for the benchmark calculations in the folder ./benchmarks/LookUp-Table. The GEM-Selektor V3 software package used to calculate the look-up table is available from http://gems.web.psi.ch. The GEM-Selektor V3 project with the thermodynamic setup and the process script is available from the last author (georg.kosakowski@psi.ch) upon request.

Competing interests

The authors declare that they have no competing interests.

Funding

The main funding is from the Helmholtz Association of German Research Centres, namely the project NUSAFE/iCross "Integrity of Nuclear Waste Repository Systems" under grant number SO-093, and also from the German Federal Ministry of Education and Research (BMBF), namely the project GeomInt "Geomechanical integrity of host and barrier rocks - experiment, modeling, and analysis of

discontinuities" under grant number 03G0866A. Partial funding comes from the Swiss National Cooperative for the Disposal of Radioactive Waste (Nagra).

Authors' contributions

Yonghui Huang implemented the look-up table approach into the OpenGeoSys software, produced simulation results of the benchmarks, and also drafted this manuscript. Georg Kosakowski designed the numerical algorithm, generated the OpenGeoSys-Gem results of the benchmarks and revised the manuscript. Haibing Shao assisted in design the numerical algorithm and contribute to the manuscript writing. Erich Wieland provided the detailed setup and properties of the generic concrete and reviewed the manuscript. Olaf Kolditz coordinated the OpenGeoSys implementation and reviewed the manuscript. All authors read and approved the final manuscript.

Acknowledgements

The first author would like to acknowledge the Chinese Scholarship Council (CSC) for financially supporting his PhD study in Germany. The authors would like to acknowledge the funding from the Helmholtz Association of German Research Centres, namely the project NUSAFE/iCross "Integrity of Nuclear Waste Repository Systems" under grant number SO-093, and also the funding from the German Federal Ministry of Education and Research (BMBF), namely the project GeomInt "Geomechanical integrity of host and barrier rocks - experiment, modeling, and analysis of discontinuities" under grant number 03G0866A. Partial financial support from the Swiss National Cooperative for the Disposal of Radioactive Waste (Nagra) is kindly acknowledged. We also thank Dr.

Ravi Patel of the Paul Scherrer Institute for helpful suggestions. We are grateful to Ms. Leslie Jakobs (UFZ, Germany) for her proof-reading and improving the language of this manuscript.

References

[1] F. Bart, F. Cau-di-Coumes, C. Frizon, S. Lorente, Cement-based materials for nuclear waste storage, Springer (2013).

[2] M. Atkins, F.P. Glasser, Application of portland cement-based materials to radioactive waste immobilization, Waste Manag. 12 (1992) 105–131. doi:10.1016/0956-053X(92)90044-J.

[3] Nagra, Vorschlag geologischer Standortgebiete für das SMA- und das HAA-Lager «Begründung der Abfallzuteilung, der Barrierensysteme und der Anforderungen an die Geologie: Bericht zur Sicherheit und Machbarkeit», (2008).

[4] R.T. Pabalan, F.P. Glasser, D. a Pickett, G.R. Walter, S. Biswas, M.R. Juckett, L.M. Sabido, J.L. Myers, Review of literature and assessment of factors relevant to performance of grouted systems for radioactive waste disposal, Contract NRC NRC-02-07-006, CNWRA. 1 (2009).

[5] W.S. Shin, The Long-Term Stability of Cement and Concrete for Nuclear Waste Disposal under Normal Geologic Conditions, (1984).

[6] G. Kosakowski, U. Berner, E. Wieland, M.A. Glaus, C. Degueldre, Geochemical evolution of the L/ILW near-field, Nagra, Wettingen, Switzerland (2014).

[7] F.P. Glasser, J. Marchand, E. Samson, Durability of concrete — Degradation phenomena involving detrimental chemical reactions, Cem. Concr. Res. 38 (2008) 226–246. doi:10.1016/j.cemconres.2007.09.015.

[8] U. Berner, Modeling the incongruent dissolution of hydrated cement minerals, Radiochem. Acta. 44 (1988) 387–393.

[9] Nagra, Effects of post-disposal gas generation in a repository for low- and intermediate-level

waste sited in the Opalinus Clay of Northern Switzerland, Nagra, Wettingen, Switzerland, (2008).

[10] G. Kosakowski, A. Jakob, AN-44-14-02 Humidity diffusion through small holes into a waste drum Georg Kosakowski, Andreas Jakob, (2014) 1–11.

[11] J.C. Walton, S. Bin-Shafique, R.W. Smith, N. Gutierrez, A. Tarquin, Role of carbonation in transient leaching of cementitious wasteforms, Environ. Sci. Technol. 31 (1997) 2345–2349. doi:10.1021/es960964j.

[12] N.R. Ravahatra, F. Duprat, F. Schoefs, T. de Larrard, E. Bastidas-Arteaga, Assessing the Capability of Analytical Carbonation Models to Propagate Uncertainties and Spatial Variability of Reinforced Concrete Structures, Front. Built Environ. 3 (2017) 1. doi:10.3389/fbuil.2017.00001.

[13] B. Šavija, M. Luković, Carbonation of cement paste: Understanding, challenges, and opportunities, Constr. Build. Mater. 117 (2016) 285–301. doi:10.1016/j.conbuildmat.2016.04.138.

[14] W. Ashraf, Carbonation of cement-based materials: Challenges and opportunities, Constr. Build. Mater. 120 (2016) 558–570. doi:10.1016/j.conbuildmat.2016.05.080.

[15] Q.T. Phung, N. Maes, D. Jacques, G. De Schutter, G. Ye, J. Perko, Modelling the carbonation of cement pastes under a CO2pressure gradient considering both diffusive and convective transport, Constr. Build. Mater. 114 (2016) 333–351. doi:10.1016/j.conbuildmat.2016.03.191.

[16] M. Thiery, G. Villain, P. Dangla, G. Platret, Investigation of the carbonation front shape on cementitious materials: Effects of the chemical kinetics, Cem. Concr. Res. 37 (2007) 1047–1058.

doi:10.1016/j.cemconres.2007.04.002.

[17] I. Yurtdas, D. Chen, D.W. Hu, J.F. Shao, Influence of alkali silica reaction (ASR) on mechanical properties of mortar, Constr. Build. Mater. 47 (2013) 165–174. doi:10.1016/j.conbuildmat.2013.04.046.

[18] N.B. Winter, Understanding Cement: An introduction to cement production, cement hydration and deleterious processes in concrete, WHD Microanalysis Consultants, Woodbridge, UK (2009).

[19] Nagra, Modellhaftes Inventar für radioaktive Materialien MIRAM 08, Nagra, Wettingen, Switzerland (2008).

[20] X. Hou, L.J. Struble, R.J. Kirkpatrick, Formation of ASR gel and the roles of C-S-H and portlandite, Cem. Concr. Res. 34 (2004) 1683–1696. doi:10.1016/j.cemconres.2004.03.026.

[21] J.L. Palandri, Y.K. Kharaka, A compilation of rate parameters of water-mineral interaction kinetics for application to geochemical modeling, U.S. Geological Survey, Menlo Park, California (2004).

[22] R. Senger, P. Marschall, S. Finsterle, Investigation of two-phase flow phenomena associated with corrosion in an SF/HLW repository in Opalinus Clay, Switzerland, Phys. Chem. Earth, Parts A/B/C. 33 (2008) S317–S326. doi:10.1016/j.pce.2008.10.034.

[23] N. Diomidis, V. Cloet, O.X. Leupin, P. Marschall, A. Poller, M. Stein, Production, consumption and transport of gases in deep geological repositories according to the Swiss disposal concept, Nagra, Wettingen, Switzerland (2016).

[24] R. Senger, J. Ewing, K. Zhang, J. Avis, P. Marschall, I. Gaus, Modeling Approaches for

Investigating Gas Migration from a Deep Low/Intermediate Level Waste Repository (Switzerland), Transp. Porous Media. 90 (2011) 113–133. doi:10.1007/s11242-010-9709-2.

[25] L. Nghiem, P. Sammon, J. Grabenstetter, H. Ohkuma, Modeling CO2 Storage in Aquifers with a Fully-Coupled Geochemical EOS Compositional Simulator, SPE/DOE Symp. Improv. Oil Recover. (2004). doi:10.2118/89474-MS.

[26] Y. Fan, L.J. Durlofsky, H.A. Tchelepi, A fully-coupled flow-reactive-transport formulation based on element conservation, with application to CO 2 storage simulations, Adv. Water Resour. 42 (2012) 47–61. doi:10.1016/j.advwatres.2012.03.012.

[27] C.I. Steefel, CrunchFlow. Software for Modeling Multicomponent Reactive Flow and Transport. User's Manual, Earth Sci. Div. Lawrence Berkeley, Natl. Lab. Berkeley, CA. Oct. (2009) 12–91.

[28] P.C. Lichtner, G.E. Hammond, C. Lu, S. Karra, G. Bisht, B. Andre, R.T. Mills, J. Kumar, J.M. Frederick, {PFLOTRAN} User Manual (2017).

[29] M.D. White, M. Oostrom, STOMP Subsurface Transport Over Multiple Phases: User`s guide, Richland, WA, 1997. doi:10.2172/553734.

[30] T. Xu, R. Senger, S. Finsterle, Corrosion-induced gas generation in a nuclear waste repository: Reactive geochemistry and multiphase flow effects, Appl. Geochemistry. 23 (2008) 3423–3433. doi:10.1016/j.apgeochem.2008.07.012.

[31] I. Sin, V. Lagneau, J. Corvisier, Integrating a compressible multicomponent two-phase flow into an existing reactive transport simulator, Adv. Water Resour. 100 (2017) 62–77. doi:10.1016/j.advwatres.2016.11.014.

[32] N. Leterrier, B. Bary, Fully Coupled Unsaturated Hydraulics and Reactive Transport Model for

the Simulation of Concrete Carbonation, J. Nucl. Res. Dev. 2 (2011) 11–18.

[33] P. Thouvenot, O. Bildstein, I. Munier, B. Cochepin, S. Poyet, X. Bourbon, E. Treille, Modeling of concrete carbonation in deep geological disposal of intermediate level waste, EPJ Web Conf. 05004 (2013) 1–8. doi:10.1051/epjconf/20135605004.

[34] L. Trotignon, P. Thouvenot, I. Munier, B. Cochepin, E. Piault, E. Treille, X. Bourbon, S. Mimid, Numerical Simulation of Atmospheric Carbonation of Concrete Components in a Deep Geological Radwaste Disposal Site During Operating Period, Nucl. Technol. 174 (2011) 424–437.

[35] D.A. Kulik, Improving the structural consistency of C-S-H solid solution thermodynamic models, Cem. Concr. Res. 41 (2011) 477–495. doi:10.1016/j.cemconres.2011.01.012.

[36] T. Matschei, D. Damidot, J. Marchand, B. Lothenbach, Thermodynamic modelling: state of knowledge and challenges, Adv. Cem. Res. 22 (2010) 211–223. doi:10.1680/adcr.2010.22.4.211.

[37] M. De Lucia, T. Kempka, M. Kühn, A coupling alternative to reactive transport simulations for long-term prediction of chemical reactions in heterogeneous CO2 storage systems, Geosci. Model Dev. 8 (2015) 279–294. doi:10.5194/gmd-8-279-2015.

[38] J.F. Lamarque, D.T. Shindell, B. Josse, P.J. Young, I. Cionni, V. Eyring, D. Bergmann, P. Cameron-Smith, W.J. Collins, R. Doherty, S. Dalsoren, G. Faluvegi, G. Folberth, S.J. Ghan, L.W. Horowitz, Y.H. Lee, I.A. MacKenzie, T. Nagashima, V. Naik, D. Plummer, M. Righi, S.T. Rumbold, M. Schulz, R.B. Skeie, D.S. Stevenson, S. Strode, K. Sudo, S. Szopa, A. Voulgarakis, G. Zeng, The atmospheric chemistry and climate model intercomparison Project (ACCMIP): Overview and description of models, simulations and climate diagnostics, Geosci. Model Dev. 6

(2013) 179–206. doi:10.5194/gmd-6-179-2013.

[39] A.M. Dunker, The Reduction and Parametrization of Chemical Mechanisms for Inclusion in Atmospheric Reaction-Transport-Models, Atmos. Environ. 20 (1985) 479–486. doi:10.1016/0004-6981(86)90088-0.

[40] K. Fukumoto, Y. Ogami, Combustion simulation technique for reducing chemical mechanisms using look-up table of chemical equilibrium calculations: Application to CO–H2–air turbulent non-premixed flame, Comput. Fluids. 66 (2012) 98–106. doi:10.1016/j.compfluid.2012.06.001.

[41] B. Fiorina, D. Veynante, S. Candel, Modeling Combustion Chemistry in Large Eddy Simulation of Turbulent Flames, Flow, Turbul. Combust. (2014) 3–42. doi:10.1007/s10494-014-9579-8.

[42] S.W. Wang, H. Levy, G. Li, H. Rabitz, Fully equivalent operational models for atmospheric chemical kinetics within global chemistry-transport models, J. Geophys. Res. 104 (1999) 30417. doi:10.1029/1999JD900830.

[43] B. Andersson, R. Andersson, L. Hakansson, M. Mortensen, R. Sudiyo, B. van Wachem, Computational Fluid Dynamics for Engineers, Cambridge University Press, 2011. doi:10.1017/CBO9781139093590.

[44] T. Turányi, A.S. Tomlin, Analysis of Kinetic Reaction Mechanisms, Springer Berlin Heidelberg, Berlin, Heidelberg, Heidelberg (2014). doi:10.1007/978-3-662-44562-4.

[45] Y. Huang, T. Nagel, H. Shao, Comparing global and local implementations of nonlinear complementary problems for the modeling of multi-component two-phase flow with phase change phenomena, Environ. Earth Sci. 76 (2017). doi:10.1007/s12665-017-6970-5.

[46] O. Kolditz, S. Bauer, L. Bilke, N. Böttcher, J.O. Delfs, T. Fischer, U.J. Görke, T. Kalbacher, G.

Kosakowski, C.I. McDermott, C.H. Park, F. Radu, K. Rink, H. Shao, H.B. Shao, F. Sun, Y.Y. Sun, A.K. Singh, J. Taron, M. Walther, W. Wang, N. Watanabe, Y. Wu, M. Xie, W. Xu, B. Zehner, OpenGeoSys: An open-source initiative for numerical simulation of thermo-hydro-mechanical/chemical (THM/C) processes in porous media, Environ. Earth Sci. 67 (2012) 589–599. doi:10.1007/s12665-012-1546-x.

[47] F. Centler, H. Shao, C. De Biase, C.H. Park, P. Regnier, O. Kolditz, M. Thullner, GeoSysBRNS-A flexible multidimensional reactive transport model for simulating biogeochemical subsurface processes, Comput. Geosci. 36 (2010) 397–405. doi:10.1016/j.cageo.2009.06.009.

[48] W. He, C. Beyer, J.H. Fleckenstein, E. Jang, O. Kolditz, D. Naumov, T. Kalbacher, A parallelization scheme to simulate reactive transport in the subsurface environment with OGS#IPhreeqc 5.5.7-3.1.2, Geosci. Model Dev. 8 (2015) 3333–3348. doi:10.5194/gmd-8-3333-2015.

[49] G. Kosakowski, N. Watanabe, OpenGeoSys-Gem: A numerical tool for calculating geochemical and porosity changes in saturated and partially saturated media, Phys. Chem. Earth. 70–71 (2014). doi:10.1016/j.pce.2013.11.008.

[50] D. Li, S. Bauer, K. Benisch, B. Graupner, C. Beyer, OpenGeoSys-ChemApp: a coupled simulator for reactive transport in multiphase systems and application to CO2 storage formation in Northern Germany, Acta Geotech. 9 (2013) 67–79. doi:10.1007/s11440-013-0234-7.

[51] R. Zolfaghari, Numerical Simulation of Reactive Transport Processes in Porous Media, Technical University Dresden (2014).

[52] B. Lothenbach, E. Wieland, A thermodynamic approach to the hydration of sulphate-resisting

Portland cement, Waste Manag. 26 (2006) 706–19. doi:10.1016/j.wasman.2006.01.023.

[53] E. Wieland, G. Kosakowski, B. Lothenbach, D.A. Kulik, Preliminary assessment of the temporal evolution of waste packages in the near field of an L/ILW repository, Nagra, Wettingen, Switzerland (2017).

[54] T. Wagner, D.A. Kulik, F.F. Hingerl, S. V. Dmytrieva, GEM-Selektor geochemical modelling package: TSolMod library and data interface for multicomponent phase models, Can. Mineral. 50 (2012) 1173–1195. doi:10.3749/canmin.50.5.1173.

[55] D.A. Kulik, T. Wagner, S. V. Dmytrieva, G. Kosakowski, F.F. Hingerl, K. V. Chudnenko, U.R. Berner, GEM-Selektor geochemical modeling package: Revised algorithm and GEMS3K numerical kernel for coupled simulation codes, Comput. Geosci. 17 (2013) 1–24. doi:10.1007/s10596-012-9310-6.

[56] W. Hummel, U. Berner, E. Curti, F. Pearson, T. Thoenen, Nagra/PSI chemical thermodynamic data base 01/01, Universal-Publishers/upublish.com, Parkland, USA (2002).

[57] B. Lothenbach, F. Winnefeld, Thermodynamic modelling of the hydration of Portland cement, Cem. Concr. Res. 36 (2006) 209–226. doi:10.1016/j.cemconres.2005.03.001.

[58] P. Blanc, A. Lassin, P. Piantone, M. Azaroual, N. Jacquemet, A. Fabbri, E.C. Gaucher, Thermoddem: A geochemical database focused on low temperature water/rock interactions and waste materials, Appl. Geochemistry. 27 (2012) 2107–2116. doi:10.1016/j.apgeochem.2012.06.002.

[59] D.A. Kulik, M. Kersten, Aqueous solubility diagrams for cementitious waste stabilization systems. 4. A carbonation model for Zn-Doped calcium silicate hydrate by Gibbs energy

minimization, Environ. Sci. Technol. 36 (2002) 2926–2931. doi:10.1021/es010250v.

[60] X. Gaona, D.A. Kulik, N. Macé, E. Wieland, Aqueous–solid solution thermodynamic model of U(VI) uptake in C–S–H phases, Appl. Geochemistry. 27 (2012) 81–95. doi:10.1016/j.apgeochem.2011.09.005.

[61] G. Kosakowski, U. Berner, The evolution of clay rock/cement interfaces in a cementitious repository for low- and intermediate level radioactive waste, Phys. Chem. Earth, Parts A/B/C. 64 (2013) 65–86. doi:10.1016/j.pce.2013.01.003.

[62] R. Dähn, A. Arakcheeva, P. Schaub, P. Pattison, G. Chapuis, D. Grolimund, E. Wieland, A. Leemann, Application of micro X-ray diffraction to investigate the reaction products formed by the alkali-silica reaction in concrete structures, Cem. Concr. Res. 79 (2016) 49–56. doi:10.1016/j.cemconres.2015.07.012.

[63] A.C. Lasaga, Chemical kinetics of water-rock interactions, J. Geophys. Res. Solid Earth. 89 (1984) 4009–4025. doi:10.1029/JB089iB06p04009.

[64] A.C. Lasaga, Fundamental approaches in describing mineral dissolution and precipitation rates, Rev. Mineral. 31 (1995) 23–86. https://ci.nii.ac.jp/naid/10025009069/en/.

[65] A.C. Lasaga, Kinetic theory in the Earth Sciences, Princeton University Press (1998). http://www.jstor.org/stable/j.ctt7zvgxm.

[66] D. Savage, C. Walker, R. Arthur, C.A. Rochelle, C. Oda, H. Takase, Alteration of bentonite by hyperalkaline fluids: A review of the role of secondary minerals, Phys. Chem. Earth, Parts A/B/C. 32 (2007) 287–297. doi:10.1016/j.pce.2005.08.048.

[67] O. Kolditz, U.-J. Görke, H. Shao, W. Wang, S. Bauer, Thermo-Hydro-Mechanical-Chemical

Processes in Fractured Porous Media: Modelling and Benchmarking, Springer International Publishing, Cham, 2015. doi:10.1007/978-3-319-11894-9.

[68] H. Hoteit, Proper Modeling of Diffusion in Fractured Reservoirs, SPE Reserv. Simul. Symp. (2011) 21–23. doi:10.2118/141937-MS.

[69] M.T. van Genuchten, A Closed-form Equation for Predicting the Hydraulic Conductivity of Unsaturated Soils1, Soil Sci. Soc. Am. J. 44 (1980) 892. doi:10.2136/sssaj1980.03615995004400050002x.

[70] J. Bear, Dynamics of Fluids in Porous Media, Courier Corporation (1972). doi:10.1097/00010694-197508000-00022.

[71] G. Kosakowski, N. Watanabe, OpenGeoSys-Gem: A numerical tool for calculating geochemical and porosity changes in saturated and partially saturated media, Phys. Chem. Earth. 70–71 (2014) 138–149. doi:10.1016/j.pce.2013.11.008.

[72] Y. Huang, O. Kolditz, H. Shao, Extending the persistent primary variable algorithm to simulate non-isothermal two-phase two-component flow with phase change phenomena, Geotherm. Energy. 3 (2015) 13. doi:10.1186/s40517-015-0030-8.

[73] B.J. Roth, Intermediate Physics for Medicine and Biology, Springer New York, New York, NY (2007). doi:10.1007/978-0-387-49885-0.

[74] J. Von Neumann, R.D. Richtmayer, A method for the numerical calculation of hydrdynamic shocks, J. Appl. Phys. 21 (1950) 232–237.

[75] Z.P. Bažant, L.J. Najjar, Nonlinear water diffusion in nonsaturated concrete, Matériaux Constr. 5 (1972) 3–20. doi:10.1007/BF02479073.

[76] P. Thouvenot, O. Bildstein, I. Munier, B. Cochepin, S. Poyet, X. Bourbon, E. Treille, Modeling of concrete carbonation in deep geological disposal of intermediate level waste, EPJ Web Conf. 05004 (2013) 1–8. doi:10.1051/epjconf/20135605004.

[77] G. Kosakowski, P. Smith, Long-term evolution of the Engineered Gas Transport System, (2014) 1–122.

[78] N.C.M. Marty, C. Tournassat, A. Burnol, E. Giffaut, E.C. Gaucher, Influence of reaction kinetics and mesh refinement on the numerical modelling of concrete/clay interactions, J. Hydrol. 364 (2009) 58–72. doi:10.1016/j.jhydrol.2008.10.013.

[79] N.I. Prasianakis, E. Curti, G. Kosakowski, J. Poonoosamy, S.V. Churakov, Deciphering pore-level precipitation mechanisms, Sci. Rep. 7 (2017). doi:10.1038/s41598-017-14142-0.

[80] Z. Bažant, L. Najjar, Nonlinear water diffusion in nonsaturated concrete, Matériaux Constr. (1972) 3–20.

[81] O. Kolditz, U.-J. Görke, H. Shao, W. Wang, S. Bauer, Thermo-hydro-mechanical-chemical processes in fractured porous media : modelling and benchmarking : Benchmarking initiatives, Springer International Publishing (2016).

[82] U. Berner, Modelling hydrated HTS cement and its pore water, Paul Scherrer Institut, Villigen, Switzerland (2009).

[83] B. Lothenbach, D.A. Kulik, T. Matschei, M. Balonis, L. Baquerizo, B.Z. Dilnesa, G.D. Miron, R.J. Myers, Cemdata18: A chemical thermodynamic database for hydrated Portland cements and alkali-activated materials, Cem. Concr. Res. (2017).

[84] D. Nied, K. Enemark-Rasmussen, E. L'Hopital, J. Skibsted, B. Lothenbach, Properties of

magnesium silicate hydrates (M-S-H), Cem. Concr. Res. 79 (2016) 323–332. doi:10.1016/j.cemconres.2015.10.003.

[85] U. Berner, D.A. Kulik, G. Kosakowski, Geochemical impact of a low-pH cement liner on the near field of a repository for spent fuel and high-level radioactive waste, Phys. Chem. Earth, Parts A/B/C. 64 (2013) 46–56. doi:10.1016/j.pce.2013.03.007.

Appendix

A. Composition of CEM I 52.5

Table A1: Composition of the cement used HTS CEM I 52.5 N according to Berner [82] **and Lothenbach and Wieland** [57]**.**

Chemical Analysis	HTS (g/100 g)	Normative composition	HTS (g/100 g)
CaO	(65.7) 66.15	Alite	61
SiO_2	22.3	Belite	18
Al_2O_3	2.7	Aluminate	3.9
Fe_2O_3	1.9	Ferrite	5.8
MgO	0.85	CaO (free)	0.45
SrO	0.16	$CaCO_3$	3.7
BaO	0.002	$MgCO_3$	n.d.
K_2O	0.22	gypsum	1.3
Na_2O[1]	(0.13) 0.19	hemihydrite	1.1
Li_2O[2]	(0.03) 0.0	anhydrite	1.5
Rb_2O[2]	(<0.001) 0.0	syngenite	n.d.
CaO (free)[3]	(0.45) 0.0	K_2SO_4	0.14
CO_2	1.6	Na_2SO_4	0.09
SO_3	2.2	K_2O	0.14
LOI[4]	1.728	Na_2O	0.09
		MgO	0.85
		SrO	0.16
		BaO	0.002

		SO_3	0.01

[1] The amount of Na_2O is increased from 0.13 % to 0.19 % in order to account for 0.03 % Li_2O (10.04 mmol/g).

[2] Li and Rb is not considered in the calculations.

[3] Free lime is added to the reactive CaO.

[4] Loss of ignition is not specified and considered as inert material (= inert quartz) in the thermodynamic model.

B. Thermodynamic setup for calculations of cement degradation

GEM-Selektor v.2-PSI: Thermodynamic data for the modelling project:

P(bar)= 1 T= 25 (°C) = 298.15 (K) RT= 2478.97

Water: Ro(g/cm3)= 0.997061 Eps= 78.2451 Visc= 0.000554753

Table B1: Thermodynamic data for Dependent Components (Species)

```
============================|=====|==========|=========|==========|======
Record Key  Name            |Flags|    gTP    |   gEx_  |   VTP    | label
============================|=====|==========|=========|==========|======
a   Al      Al(SO4)+         d + +    -1250429         0    -0.6019
a   Al      Al(SO4)2-        d + +    -2006304         0     3.1112
a   Al      Al+3             d + +     -483708         0    -4.5243
a   Al      AlO+             d + +     -660420         0     0.0307
a   Al      AlO2-            d + +     -827479         0     0.9467
a   Al      AlO2H@           d + +     -864277         0     1.3009
a   Al      AlOH+2           d + +     -692595         0    -0.2728
```

	a	AlSi	AlHSiO3+2	r + +	-1540546	0	0.0000
1235	a	Ba	Ba(CO3)@	d + +	-1104251	0	-1.1799
	a	Ba	Ba(HCO3)+	d + +	-1153325	0	1.9172
	a	Ba	Ba(SO4)@	d + +	-1320652	0	0.8182
	a	Ba	Ba+2	d + +	-560782	0	-1.2901
	a	Ba	BaOH+	d + +	-721077	0	0.9159
1240	a	Ca	Ca(CO3)@	d + +	-1099176	0	-1.5648
	a	Ca	Ca(HCO3)+	d + +	-1146041	0	1.3330
	a	Ca	Ca(SO4)@	d + +	-1310378	0	0.4701
	a	Ca	Ca+2	d + +	-552790	0	-1.8439
	a	Ca	CaOH+	d + +	-717024	0	0.5762
1245	a	CaSi	Ca(HSiO3)+	d + +	-1574238	0	-0.6737
	a	CaSi	CaSiO3@	r + +	-1517557	0	0.0000
	a	Fe+2	Fe(CO3)@	d + +	-644487	0	-1.7228
	a	Fe+2	Fe(HCO3)+	d + +	-689860	0	0.8184
	a	Fe+2	Fe(HSO4)+	d + +	-853475	0	1.8806
1250	a	Fe+2	Fe(SO4)@	d + +	-848806	0	0.1672
	a	Fe+2	Fe+2	d + +	-91504	0	-2.2640
	a	Fe+2	FeCl+	d + +	-223593	0	0.0846
	a	Fe+2	FeOH+	d + +	-274461	0	-1.6713
	a	Fe+3	Fe(HSO4)+2	d + +	-787148	0	0.2320
1255	a	Fe+3	Fe(SO4)+	d + +	-784705	0	-0.2635
	a	Fe+3	Fe(SO4)2-	d + +	-1536813	0	3.0485
	a	Fe+3	Fe+3	d + +	-17185	0	-3.7790
	a	Fe+3	Fe2(OH)2+4	r + +	-491897	0	0.0000
	a	Fe+3	Fe3(OH)4+5	r + +	-964326	0	0.0000
1260	a	Fe+3	FeCl+2	d + +	-156923	0	-2.2857
	a	Fe+3	FeCl2+	d + +	-291923	0	1.0272
	a	Fe+3	FeCl3@	d + +	-417505	0	3.5941

	a	Fe+3	FeO+	d + +	-222004	0	-4.2021
	a	Fe+3	FeO2-	d + +	-368258	0	0.0452
1265	a	Fe+3	FeO2H@	d + +	-419858	0	0.7209
	a	Fe+3	FeOH+2	d + +	-241868	0	-2.5341
	a	Fe+3Si	FeHSiO3+2	r + +	-1087151	0	0.0000
	a	K	K(SO4)-	d + +	-1031773	0	2.7464
	a	K	K+	d + +	-282462	0	0.9009
1270	a	K	KOH@	d + +	-437107	0	1.4965
	a	Mg	Mg(CO3)@	d + +	-998975	0	-1.6776
	a	Mg	Mg(HCO3)+	d + +	-1047022	0	0.9343
	a	Mg	Mg+2	d + +	-453985	0	-2.2014
	a	Mg	MgOH+	d + +	-625868	0	0.1641
1275	a	Mg	MgSO4@	d + +	-1211972	0	0.1812
	a	MgSi	Mg(HSiO3)+	d + +	-1477145	0	-1.0850
	a	MgSi	MgSiO3@	r + +	-1425030	0	-0.0002
	a	Na	Na(CO3)-	d + +	-797112	0	-0.0421
	a	Na	Na(HCO3)@	d + +	-847394	0	3.2318
1280	a	Na	Na(SO4)-	d + +	-1010336	0	1.8640
	a	Na	Na+	d + +	-261881	0	-0.1208
	a	Na	NaOH@	d + +	-418124	0	0.3509
	a	Si	HSiO3-	d + +	-1014598	0	0.4526
	a	Si	Si4O10-4	r + +	-3600807	0	-0.0008
1285	a	Si	SiO2@	d + +	-833411	0	1.6063
	a	Si	SiO3-2	r + +	-938510	0	-0.0002
	a	Sr	Sr(CO3)@	d + +	-1107830	0	-1.5228
	a	Sr	Sr(HCO3)+	d + +	-1157538	0	1.4082
	a	Sr	Sr(SO4)@	d + +	-1321366	0	0.5025
1290	a	Sr	Sr+2	d + +	-563836	0	-1.7758
	a	Sr	SrOH+	d + +	-725159	0	0.7099

```
      a   wC+4     CO2@              d + +     -386015         0     3.2807
      a   wC+4     CO3-2             d + +     -527982         0    -0.6058
      a   wC+4     HCO3-             d + +     -586940         0     2.4211
1295  a   wC-4     CH4@              d + +      -34354         0     3.7398
      a   wCl+7    ClO4-             d + +       -8535         0     4.3904
      a   wCl-1    Cl-               d + +     -131290         0     1.7341
      a   wH0      H2@               d + +       17729         0     2.5264
      a   wO0      O2@               d + +       16446         0     3.0501
1300  a   wS+2     S2O3-2            d + +     -519989         0     2.7592
      a   wS+4     HSO3-             d + +     -529098         0     3.2957
      a   wS+4     SO3-2             d + +     -487886         0    -0.4116
      a   wS+6     HSO4-             d + +     -755805         0     3.4841
      a   wS+6     SO4-2             d + +     -744459         0     1.2918
1305  a   wS-2     H2S@              d + +      -27930         0     3.4951
      a   wS-2     HS-               d + +       11969         0     2.0210
      a   wS-2     S-2               r + +      120422         0     0.0000
      a   wX       OH-               d + +     -157270         0    -0.4708
      a   w_       H+                d + +           0         0     0.0000
1310  a   w_       H2O@              d + +     -237181         0     1.8068
      g   C+4      CO2               d + +     -394393         0  2478.9712
      g   C-4      CH4               d + +      -50659         0  2478.9712
      g   H0       H2                d + +           0         0  2478.9712
      g   O0       O2                d + +           0         0  2478.9712
1315  g   S-2      H2S               d + +      -33752         0  2478.9712
      s   CaAlSiOH C3AS0.84H4.3_05   d + +    -2682620         0     7.1246  1
      s   CaFeSiOH C3FS0.84H4.3_05   d + +    -2239950         0     7.4261  1
      s   CaSiOH   ECSH2-JenCa       r + +    -1570649         0     4.7477  2
      s   CaSiOH   ECSH2-TobCa       r + +    -1834325         0     5.7590  2
1320  s   KSiOH    ECSH2-KSH         r + +     -440835         0     2.9665  2
```

	s	NaSiOH	ECSH2-NaSH	r	+	+	-431229	0	2.4557	2
	s	SrSiOH	ECSH2-SrSH	r	+	+	-2021120	0	6.1810	2
	s	MgAlCOH	Mg3AlC0.5OH	d	+	+	-4339850	0	11.4960	1
	s	MgFeCOH	Mg3FeC0.5OH	d	+	+	-3882600	0	11.9040	1
1325	s	MgSiOH	M3S2H5	r	+	e	-4715611	0	14.8600	3
	s	MgSiOH	M3S4H5	r	+	e	-6442367	0	18.9800	3
	s	AlOH	Gibbsite	d	+	+	-1150986	0	3.1956	
	s	NaAlSiO	Albite(low)	r	+	e	-3704514	0	10.0070	
	s	FeAlSiOH	Chamosite	r	+	e	-6499558	0	21.5880	4
1330	s	KAlSiOH	Illite(Mg)	r	+	e	-5501960	0	14.0070	4
	s	NaAlSiOH	Analcime	r	+	e	-3082123	0	9.7090	4
	s	CaAlSiOH	Chabazite	r	+	e	-7159841	0	25.1160	4
	s	NaAlSiOH	ClinoptiloliteNa	r	+	e	-6256557	0	21.4780	4
	s	AlSiOH	Kaolinite	r	+	e	-3783140	0	9.9340	4
1335	s	CaAlSiOH	Laumontite	r	+	e	-6684590	0	20.7530	4
	s	NaAlSiOH	Montmor-MgNa	r	+	e	-5309924	0	13.3980	4
	s	CaAlSiOH	Mordenite	r	+	e	-6165480	0	20.9800	4
	s	NaAlSiOH	Natrolite	r	+	e	-5304184	0	16.9200	4
	s	CaAlSiOH	Phillipsite_Ca	r	+	e	-4432975	5708	15.1150	4
1340	s	KAlSiOH	Phillipsite_K	r	+	e	-4452053	5708	14.8970	4
	s	NaAlSiOH	Phillipsite_Na	r	+	e	-4423354	5708	14.9690	4
	s	CaAlSiOH	Scolecite	r	+	e	-5585717	0	17.2300	4
	s	BaCO	Witherite	r	+	+	-1137635	0	4.4080	
	s	BaSO	Brt	d	+	+	-1362152	0	5.2100	
1345	s	CaSiO	C2S	d	+	+	-2193211	0	5.1790	
	s	CaAlO	C3A	d	+	+	-3382346	0	8.9217	
	s	CaSiO	C3S	d	+	+	-2784326	0	7.3180	
	s	CaAlFeO	C4AF	d	+	+	-4786496	0	13.0202	
	s	CaAlOH	C2AH7.5	d	+	+	-4695538	0	17.9710	

1350	s	CaAlOH	C3AH6	d	+	+	-5008155	0	14.9702	
	s	CaAlOH	C4AH13	d	+	+	-7324269	0	27.3980	
	s	CaAlOH	C4AH19	d	+	+	-8749936	0	37.0872	
	s	CaAlOH	CAH10	d	+	+	-4622959	0	19.3985	
	s	CaAlOsH	Monosulphate	d	+	+	-7778504	0	30.9030	
1355	s	CaAlOSH	Straetlingite	d	+	+	-5705148	0	21.6110	
	s	CaAlOcH	Hemicarbonate	d	+	+	-7335973	0	28.4515	
	s	CaAlOcH	Monocarbonate	d	+	+	-7337459	0	26.1958	
	s	CaClH10	C4AClH10	d	+	+	-6810900	0	27.2300	
	s	CaClSO4H	C4AsClH12	d	+	+	-7533398	0	28.8600	
1360	s	CaAlOsH	Ettringite	d	+	+	-15205936	0	70.7030	
	s	CaCO	Calcite	d	+	+	-1129176	0	3.6934	
	s	CaFeOcH	Fe-hemicarbonate	d	+	+	-5952868	0	27.3393	
	s	CaFeOcH	Femonocarbonate	d	+	+	-6674009	0	29.1666	
	s	CaMgCO	Dolomite (ord)	d	+	+	-2160289	0	6.4340	
1365	s	CaOH	Portlandite	d	+	+	-897013	0	3.3060	
	s	CaSO	Gypsum	d	+	+	-1797763	0	7.4690	
	s	FeCO	Siderite	d	+	+	-681647	0	2.9378	
	s	FeO	Hydro-magnetite	r	+	+	-1468946	0	11.6180	5
	s	FeO	Magnetite	d	+	+	-1017412	0	4.4524	
1370	s	FeOH	FeOOH_mic	d	+	+	-480136	0	3.4306	
	s	FeS	Pyrite	d	+	+	-173165	0	2.3940	
	s	CaKSOH	Syngenite	d	+	+	-2884913	0	12.7540	
	s	MgAlOH	Hydrotalcite	d	+	+	-6394560	0	22.0200	
	s	MgCO	Magnesite	d	+	+	-1029275	0	2.8020	
1375	s	MgO	Periclase	r	+	+	-567931	0	1.1246	
	s	MgOH	Brucite	d	+	+	-832227	0	2.4630	
	s	SiO	Inert_Qtz	d	+	+	-854793	0	2.2688	6
	s	SiO	Quartz	d	+	+	-854793	0	2.2688	7

```
      s   SiO     Amorphous silica d + +     -848903         0     2.9000  8
1380  s   SrCO    Strotianite      d + +    -1144735         0     3.9010
      s   SrSO    Celestite        d + +    -1346150         0     4.6250
      ============================|=====|==========|=========|==========
      Molar Gibbs energies are in J/mol, volumes in J/bar (0.1 cm3/mol).
      Flags: first column - data source (d-DComp, r-ReacDC);
1385  second column - on/off in the current system definition;
      third column - within (+) or out of (e) the source TP intervals.

      ------
```

1390 Labels:

1: The two components define an ideal solid solution phase.

2: The components form an ideal solid solution phase for C-S-H with alkali uptake according to Lothenbach et al. [83].

3: The two components form an ideal solid solution for M-S-H according to Nied et al. [84].

1395 4: The clay and zeolite phases in this setup are imported from Thermoddem DB [58].

5: Definition of hydro-magnetite according to Berner et al. [85]

6: This phase represents an inert mineral phase with the properties identical to quartz.

7: This (kinetically controlled) phase is used to represent the quartz aggregate.

8: Amorphous silica is in some realizations used to allow for precipitation of SiO_2 (see text).